Journal of King Saud University – Science 34 (2022) 102350

HOSTED BY

Contents lists available at ScienceDirect

Journal of King Saud University – Science

journal homepage: www.sciencedirect.com

Original article

Hydrogen bonds interactions in biuret-water clusters: FTIR, X-ray diffraction, AIM, DFT, RDG, ELF, NLO analysis

Aleksandr S. Kazachenko [a,b,c,*], Noureddine Issaoui [d], Abir Sagaama [d], Yuriy N. Malyar [a,b], Omar Al-Dossary [e,*], Leda G. Bousiakou [f], Anna S. Kazachenko [a], Angelina V. Miroshnokova [a,b], Zhouyang Xiang [g]

[a] Siberian Federal University, pr. Svobodny, 79, Krasnoyarsk 660041, Russia
[b] Institute of Chemistry and Chemical Technology, Krasnoyarsk Science Center, Siberian Branch, Russian Academy of Sciences, Akademgorodok, 50/24, Krasnoyarsk 660036, Russia
[c] Prof. V.F. Voino-Yasenetsky Krasnoyarsk State Medical University of the Ministry of Healthcare of the Russian Federation, St. Partizan Zheleznyak, Bld. 1, Krasnoyarsk 660022, Russia
[d] Laboratory of Quantum and Statistical Physics (LR18ES18), Faculty of Sciences, University of Monastir, Monastir 5079 Tunisia
[e] Department of Physics and Astronomy, College of Science, King Saud University, PO Box 2455, Riyadh 11451, Saudi Arabia
[f] IMD Laboratories Co, R&D Section, Lefkippos Technology Park, NCSR Demokritos PO Box 60037, 15130 Athens, Greece
[g] State Key Laboratory of Pulp and Paper Engineering, South China University of Technology, Guangzhou 510640, China

ARTICLE INFO

Article history:
Received 30 May 2022
Revised 18 September 2022
Accepted 28 September 2022
Available online 7 October 2022

Keywords:
Biuret
Clusters
Water
DFT
QTAIM
RDG

ABSTRACT

In this work, we studied intermolecular aqueous clusters of biuret, an important urea derivative. FTIR showed an increase in the intensity of absorption bands when water molecules are introduced into the biuret. X-ray diffraction analysis showed that the introduction of water molecules into the biuret structure significantly increases the intensity of the bands on the diffraction patterns in the range from 14 to 65 2θ. Aqueous biuret clusters have also been studied in the gas phase by theoretical methods: density functional theory and Atoms in Molecules (AIM) using the DFT level B3LYP/6–31 + G (d, p). The nature of molecular interactions between water and biuret through hydrogen bonds was also investigated using the electron localization function (ELF) and non-covalent reduced density gradient (NC-RDG). The thermodynamic and Non-linear optical properties of biuret-water clusters were performed also.

1. Introduction

Urea is recognized as the first artificially synthesized organic molecule (Yokoya et al., 2021). This discovery provided an opportunity for the development of the field of synthetic organic chemistry, and the synthesis of very complex and / or strained molecules became possible (Nicolaou et al., 2005).

Urea derivatives using in engineering and chemical-catalytic processes (Bernhard et al., 2012), due to the increased use of urea as a reducing agent for the selective catalytic reduction of nitrogen oxides in the after treatment of diesel engine exhaust gases (Koebel et al., 2000), and new materials (Dong et al., 2011), due to recent studies of urea derivatives as precursors of carbon nitride materials (Liu et al., 2011).

Biuret (carbamylurea) is a chemical compound with the chemical formula $[H_2NC(O)]_2NH$, formed as a result of the condensation of two equivalents of urea (Hughes et al., 1961). Biuret is also used as a non-protein nitrogen source in ruminant feed (Kunkle et al., 2013), where it is converted to protein by intestinal microorganisms. (Oltjen et al., 1969) It is less preferred than urea due to its higher cost and lower digestibility, but the latter characteristic also slows down its digestion and thus reduces the risk of ammonia poisoning (Fonnesbeck et al., 1975).

In recent studies (Kazachenko et al., 2021), biuret has been investigated as a catalyst for the sulfation of polysaccharides with sulfamic acid, as an alternative to urea.

In aqueous solutions, the phenomenon of clustering of some organic and inorganic molecules is encountered, which has recently been actively studied, both theoretically and experimentally (Akman et al., 2020; Kazachenko et al., 2021). Water clusters

* Corresponding authors at: Siberian Federal University, pr. Svobodny, 79, Krasnoyarsk 660041, Russia.
E-mail addresses: leo_lion_leo@mail.ru, kazachenko.as@icct.krasn.ru (A.S. Kazachenko), omar@ksu.edu.sa (O. Al-Dossary).
Peer review under responsibility of King Saud University.

Production and hosting by Elsevier

https://doi.org/10.1016/j.jksus.2022.102350
1018-3647/

are discrete hydrogen-bonded assemblies or clusters of molecules in water (Ludwig, 2001).

Water clusters of various classes of substances have been actively studied in recent years. Thus, water clusters of ozone in various water/ozone ratios were studied in (Yadav et al., 2017), and the maximum binding capacity of water clusters of various sizes with respect to ozone molecules was shown. In (Wang et al., 2015), the interaction of new polymers with a water cluster was studied. Water clusters in crystalline hydrates were studied in (Supriya and Das, 2003). In (Akman et al., 2020), aqueous thiourea clusters were studied by both experimental and theoretical methods. A similar work was presented for ammonium sulfamate (Kazachenko et al., 2021) and sulfamic acid (Kazachenko et al., 2022). It is shown that despite the similarity of the structure of ammonium sulfamate and sulfamic acid, their clustering with water occurs differently, which is affected by the presence of the ammonium cation in the sulfamate. The influence of urea on water, including in clusters, was actively studied by experimental and theoretical methods in (Lovrinčević et al., 2020; Carr et al., 2013) and others.

Based on all of the above, the importance of studying water clusters of various substances is obvious. This work is a systematic continuation of the previously started topic of the study of water clusters of some acids, salts and urea derivatives. In this regard, the combined use of experimental and theoretical methods allows us to obtain the most reliable picture.

In this work, we studied aqueous clusters of biuret by FTIR, X-ray diffraction, QTAIM, DFT, RDG, ELF, NLO.

2. Experimental

2.1. FTIR and XRD analysis

Samples of the Biuret-water cluster were obtained by dissolving biuret in distilled water at 70C, followed by precipitation of the cluster at room temperature.

Shimadzu IR Tracer-100 spectrometer (Japan) within the wavelength range of 400–4000 cm^{-1} was used for registration FTIR spectra of biuret and biuret-water cluster. OPUS program (version 5.0) was used for analysis spectral data. Solid samples for analysis were prepared in the form of pills in a KBr matrix (2 mg sample/1000 mg KBr).

DRON-3 X-ray diffractometer (CuKα monochromatized radiation (λ = 0.154 nm), voltage 30 kV, current 25 mA) was used for X-ray diffraction (XRD) phase analysis. The scanning step is 0.02 deg; intervals for 1 s per data point. The measurement was carried out in the interval of the Bragg angles 2Θ from 5.00 to 70.00 deg.

2.2. Computational details

Molecular stability of each biuret-Water cluster has been investigated by calculating the SCF energy of these different structures. The calculation was performed using B3LYP/6–31 + G(d,p) method via Gaussian 09 software (Frisch et al., 2013). The output of various theories shows similar results but DFT theory results was more accurate compared with experimental data, so we are mentioning the results of DFT theory only. DFT theory is an effective tool for performing chemical calculations of compounds, better representation of polar bonds and accretion of lower basis set can also be done (Petersson and Al-Laham, 1991; Petersson et al., 1988). The initial configuration searches for the biuret-water clusters were based on two steps. Firstly, the isomer component of the ABCluster software (Zhang and Dolg, 2015) was used to generate the initial structures of biuret water clusters. Both 2D and 3D initial guesses have been considered to make sure we get the true global minima of each structure. Secondly, Each of the generated structure was then fully optimized by DFT using B3LYP functional with the polarized basis sets (6–31 + G(d,p)) by Gaussian 09 package to obtain the respective total energy and locate the most stable geometry for each cluster. The optimized geometry of the considered clusters was confirmed to be located at the local true minima on the potential energy surface, as indicated by the lack of imaginary frequencies in the vibrational mode calculation. In addition, molecular electrostatic potential (MEP) surface was plotted for the considered clusters by using B3LYP/6–31 + G(d,p) level of theory. The MEP and all the output files were visualized by means of GaussView software (Dennington et al., 2010). The important parameters was the energy gap which considered the differences between the lowest unoccupied molecular orbital (LUMO) and the highest occupied molecular orbital (HOMO). This gap gives the stability and tells about hard and soft nature of cluster. Then, topological analysis was carried out to discover the non covalent interactions. The wavefunctions obtained at the B3LYP/6–31 + G(d,p) level were used to determine the electron density ρ_c and the Laplacien electron density ($\nabla^2\rho_c$) at the bond critical points (BCPs). The AIM, RDG and ELF visual representations were generated throughout Multiwfn 3.8 program (Lu and Chen, 2012).

3. Results and discussions

3.1. FTIR and XRD analysis

The initial biuret and its water clusters were analyzed by FTIR spectroscopy (Fig. 1).

Fig. 1 shows the spectra of biuret and water biuret cluster. Basic infrared spectral data of biuret and its water cluster are presented in Table 1.

In the spectra of biuret and its water cluster, two bands are observed (3200–3420 cm^{-1}) in the region of stretching vibrations of N—H. The former is alternatively referred to as bridging hydroxide, while the band of water hydration appears at about 3420 cm^{-1} (Wang et al., 2016). Bending N — H vibrations are observed at 1585 cm^{-1} with significant intensity. It is reported that the frequencies of carbonyl stretching vibrations in compounds containing the CO-NH-CO group give two bands (Uno and Machida, 1962); the peak of the asymmetric stretching vibration appears above 1720 cm^{-1}, and the peak of the symmetric vibration appears at about 1680–1695 cm^{-1} (Hajji et al., 2021; Hajji et al., 2021).

When coordination occurs, it determines the degree of electron delocalization in the *N*-CO-N system; thus, coordination through the oxygen atom will lead to a decrease in the nature of the double bond of the C═O bonds and will lead to a shift in the carbonyl extension mode to the region of lower frequencies (Udupa and Indira, 1975).

The peaks of stretching vibrations of C═O bonds are found at 1684, 1693, 1622 cm^{-1}, respectively.

The peaks of bending vibrations of C═O bonds, found in the region of 624–671 cm^{-1}, may indicate some coordination between water models and oxygen atoms in biuret.

In addition, for the aqueous biuret cluster, there is a significant increase in the signal intensity of almost all absorption bands in comparison with the initial biuret, which is consistent with the data (Akman et al., 2020; Kazachenko et al., 2021). The peak of intermolecular hydrogen bonds of OH groups is observed at 3500–3200 cm^{-1}, and its intensity increases by about 5 times when passing from biuret to an aqueous biuret cluster.

According to Fig. 2, the background of the X-ray diffraction patterns is low, and the diffraction intensity is high, which indicates that the complex has a fine-crystalline state. The X-ray diffraction

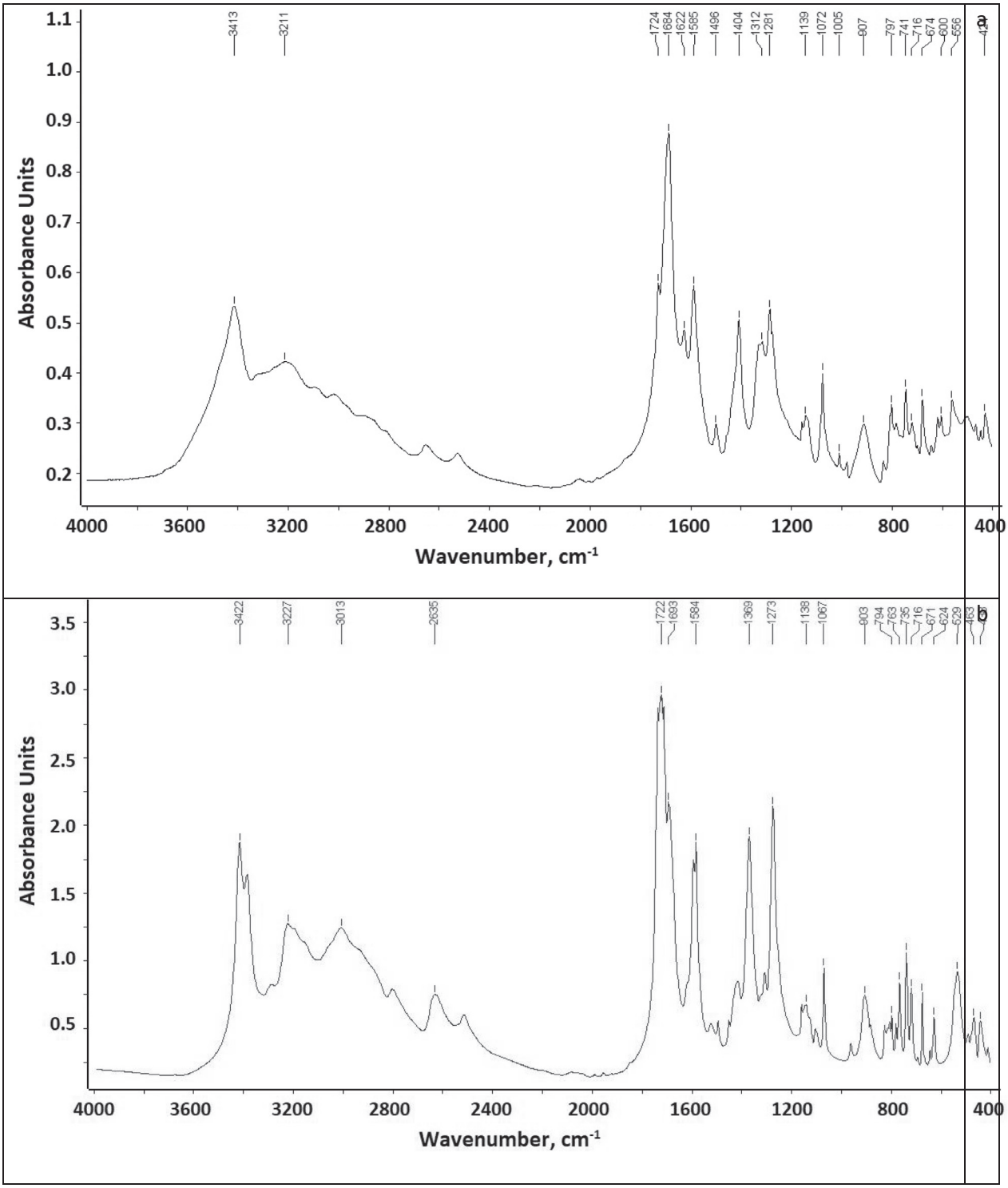

Fig. 1. FTIR spectra: a - Biuret, b - Biuret water cluster.

pattern of the original biuret has high intensity bands at 11,15,17,19,21,23,29,39 2⊖ (deg), which corresponds to the data given in (Udachin et al., 2011).

The inclusion of water molecules in the biuret crystal leads to a significant increase in the intensity of most peaks in the range from 14 to 65 2⊖ (deg). A similar phenomenon was observed for thiourea (Akman et al., 2020), ammonium sulfamate (Kazachenko et al., 2021), which can also be explained by the specific effect of water molecules on the crystal structure of compounds (Volz and Clayden, 2011).

3.2. Structural analysis of Biuret -$(H2O)_n$ clusters (n = 1–10)

Urea and its derivatives, which have both acceptor and donor parts of the hydrogen bond, are an ideal structure for the formation of various intermolecular clusters (Yokoya et al., 2021), including

Table 1
Assignment of absorption bands in the FTIR spectra of biuret and water biuret cluster.

Wavenumber, cm^{-1}		Vibration type
Biuret	Biuret-water	
3413	3422	ν_{as} (NH_2) + ν(H_2O)/ν_{as}(NH_2)
3211	3227	ν_{as}(NH_2)
1724	1722	ν(C═O)
1585	1584	δ(NH_2)
1496, 1404	1369	ν(C—N) + ν(C − NH_2)
1281	1273	δ(N—H)
1139	1138	ν(C—N) + δ(N—H)
1072	1067	ν(C—N)
907	903	ν(C—N) + ν(C − NH_2)
797	794	δ(C − NH_2)
716	716	δ(C═O)

water clusters (Akman et al., 2020). Recently, urea derivatives have attracted particular attention due to the fact that they contain important functional groups (Hammami et al., 2015).

To determine the interactions of the biuret molecule in water, the most stable clusters of biuret with water were identified. The most stable clusters are possible, such as Biuret -(H_2O), Biuret -(H_2O)$_2$, Biuret -(H_2O)$_3$, Biuret -(H_2O)$_4$, Biuret -(H_2O)$_5$, Biuret -(H_2O)$_6$, Biuret -(H_2O)$_7$, Biuret -(H_2O)$_8$, Biuret-(H_2O)$_9$, Biuret-(H_2O)$_{10}$, have been optimized at the level of B3LYP theory with a 6–31 + G (d, p) basis set and are represented by atomic numbers in Fig. 3 (a-l).

The optimized parameter such as bond lengths of Biuret-(H_2O)$_{(1-10)}$ clusters were computed using the B3LYP theory with a 6–31 + G (d, p) method and compared with each other. The optimized bond parameters of the biuret water clusters (Biuret-(H_2O)$_{(1-10)}$) are shown in Table 2 and 3.

According to the data given in Tables 2 and 3, the bond lengths C1-N8, *C*2-O10, H4-N8, H5-N9, O13-H15 in a cluster of water biuret with one water molecule (Biuret- (H_2O)) are slightly longer than in other water clusters, while the lengths of the *C*2-N9, *C*2-O12, C1-O11, and H3-N8 bonds in the Biuret- (H_2O) cluster are shorter than in other clusters, that these bonds may be associated with greater sensitivity to hydration (Akman et al., 2020; Kazachenko et al., 2021).

The shortest bond length with a value of 0.9613 Å is observed for O1-H2 in the Biuret- (H_2O)$_3$ cluster. It should also be noted that a group of OH bonds with rather low values is observed for the Biuret- (H_2O) $_5$ cluster: O22-H23 (0.9645 Å), O22-H24 (0.9903 Å), O25-H26 (0.9636 Å), and O25-H27 (0.9893 Å). The longest bond lengths H8-H14 (2.0819 Å) and O21-H24 (2.0134 Å) are observed for the Biuret cluster - (H_2O) $_6$, H39-O40 (2.0021 Å) for the Biuret - (H_2O) $_{10}$ cluster.

In the Biuret-(H_2O)cluster (Fig. 3a, Table 4), the bonding energy is −58.45 kJ/mol (Table 5), and its is formed by one hydrogen bonds, such as, O13-H15…O12 with values X-H··· X 1.867. In the Biuret-(H_2O)$_2$cluster (Fig. 3b), the bonding energy is −111.45 kJ/-mol, and its structure is formed by two hydrogen bonds, such as, O16- H17…O12, O13-H14…O16with values X-H··· X:1.750, 1.740, respectively. In the Biuret-(H_2O)$_3$ cluster (Fig. 3c), the bonding energy is −636.45 kJ/mol, and its structure is formed by three hydrogen bonds, such as, O4-H14…O16, O1-H3…O4, O19-H21…O1with values X-H··· X:1.74, 1.72, 1.71, respectively. It should be noted that the ring structure for aqueous biuret complexes is formed only for clusters with four water molecules and higher. In the Biuret-(H_2O)$_4$ cluster (Fig. 3d), the bonding energy is −242.45 kJ/mol, and its structure is formed by five hydrogen bonds, such as, O22-H24…O12, O16-H18…O22, O19-H21…O16, O13-H15…O22, O19-H20…O13 with values X-H··· X:1.64, 1.87, 1.85, 1.85, 1.88, respectively. In the Biuret-(H_2O)$_5$cluster (Fig. 3e), the bonding energy is −294.45 kJ/mol, and its ring structure is formed by six hydrogen bonds, such as, O1-H3…O18, O19-H20…O18, O22-H24…O1, O4-H5…O22, O4-H6…O25, O25-H27…O19with values X-H··· X:1.76, 1.96, 1.73, 1.95, 1.79, 1.75, respectively. In the Biuret-(H_2O)$_6$ cluster (Fig. 3f), the bonding energy is −347.45 kJ/mol, and its ring structure is formed by elevenhydrogen bonds, such as, N18-H14…O7, N18-H14…O8, O7-H9…O4, O1-H2…O4, O25-H27…O1, O28-H29…O25, O22-H23…O25, O4-H6…O28, O28-H30…O21, O22-H24…O21, O7-H8…O22 with values X-H··· X:1.82, 2.01, 1.93, 1.79, 1.73, 1.94, 1.93, 1.64, 1.86, 2.01, 1.83, respectively. In the Biuret-(H_2O)$_7$ cluster (Fig. 3g), the bonding energy is −426.45 kJ/mol, and its ring structure is formed by twelve hydrogen bonds, such as, N18-H14…O7, O7-H8…O31, O25-H27…O31, O4-H5…O21, O22-H23…O21, O31-H33…O4, O4-H6…O28, O22-H24…O28, O28-H29…O25, O25-H27…O31, O25-H26…O1, O1-H2…O22 with values X-H··· X:1.87, 1.85, 1.92, 1.88, 1.88, 1.65, 1.90, 1.96, 1.68, 1.92, 1.92, 1.65, respectively. In the Biuret-(H_2O)$_8$ cluster (Fig. 3h), the bonding energy is −478.45 kJ/mol, and its ring structure is formed by twelve hydrogen bonds, such as, O1-H2…O24, O4-H5…O24, O4-H6…O25, O25-H27…O31, O31-H32…O34, O10-*H*11…O7, O31-H33…O7, O10-H12…O34, O7-H9…O1, O1-H3…O25, O34-H35…O28, O28-H29…O4with values X-H··· X:1.87, 1.88, 1.87, 1.67, 1.88, 1.84, 1.91, 1.85, 1.64, 1.89, 1.64, 1.65, respectively. In the Biuret-(H_2O)$_9$ cluster (Fig. 3i), the bonding energy is −556.45 kJ/mol, and its ring structure is formed by fourteen hydrogen bonds, such as, O4-H6…O24, O1-H2…O4, O28-H30…O24, N21-H17…O25, O25-H27…O34, O28-H29…O34, O7-H9…O28, O34-H36…O31, O1-H3…O10, O31-H32…O10, O10-*H*11…O37, O37-H38…O4, O37-H39…O7, O25-H26…O1with values X-H··· X:1.74, 1.94, 1.88, 1.80, 1.85, 1.89, 1.65, 1.64, 1.91, 1.87, 1.65, 1.88, 1.85, 1.74, respectively. In the Biuret-(H_2O)$_{10}$cluster (Fig. 3j), the bonding energy is −583.45 kJ/mol, and its ring structure is formed by fifteen hydrogen bonds, such as, O37-H38…O27, O37-H39…O40, O7-H9…O37, O1-H2…O7, O1-H3…O40, O13-H14…O1, O28-H29…O10, O28-H30…O34, O40-H42…O34, O34-H35…O4, O4-H5…O31, O13-H15…O31, O31-H32…O28, O10-H12…O13, O4-H6…O1 with values X-H··· X:1.96, 2.00, 1.75, 1.80, 1.79, 1.73, 1.99, 1.90, 1.96, 1.69, 1.95, 1.86, 1.67, 1.89, 1.92, respectively.

Hydrogen bonds O ··· O between water molecules are also observed and, as was found, are shorter than hydrogen bonds NH … O, which indicates that the cyclic parts of aqueous biuret clusters with 6 (or more) water molecules are especially stabilized by OH … O hydrogen bonds, which is consistent with (Zumdahl, 2000). DFT calculations for aqueous biuret clusters with 6 (or more) water molecules show that a probable cluster is stabilized due to the formation of a ring structure around some parts of the central biuret molecule.

Intermolecular interaction energies of with hydrogen bonds calculated by the B3LYP / 6–31 + G (d, p) method (Table 4). The energies of intermolecular interaction with hydrogen bonds in the biuret water clusters calculated by the formula:

$$\Delta E = E(\text{cluster})-[E(\text{Biuret}) + n^{*}E(H2O)] \quad (1).$$

According to Table 5, the minimum value of Bonding energy (-58.45 kJ / mol) is observed for an aqueous biuret cluster with one water molecule. It should be noted that the maximum value of Bonding energy (-636.45 kJ / mol) is observed for the Biuret-(H_2O) $_3$ cluster, which may be associated with some energy intensity of this structure. The ring structure is observed in Biuret-(H_2O)$_n$ (n = 4–10). Bonding energy values for these clusters change almost linearly from R^2 = 0.9924 (Fig. 4).

For all water clusters of biuret, starting from Biuret- (H_2O), with an increase in the number of molecules in the cluster, there is a linear change in the Energy value from −1235219 to −3041747 kJ / mol (Fig. 4, Table 5).

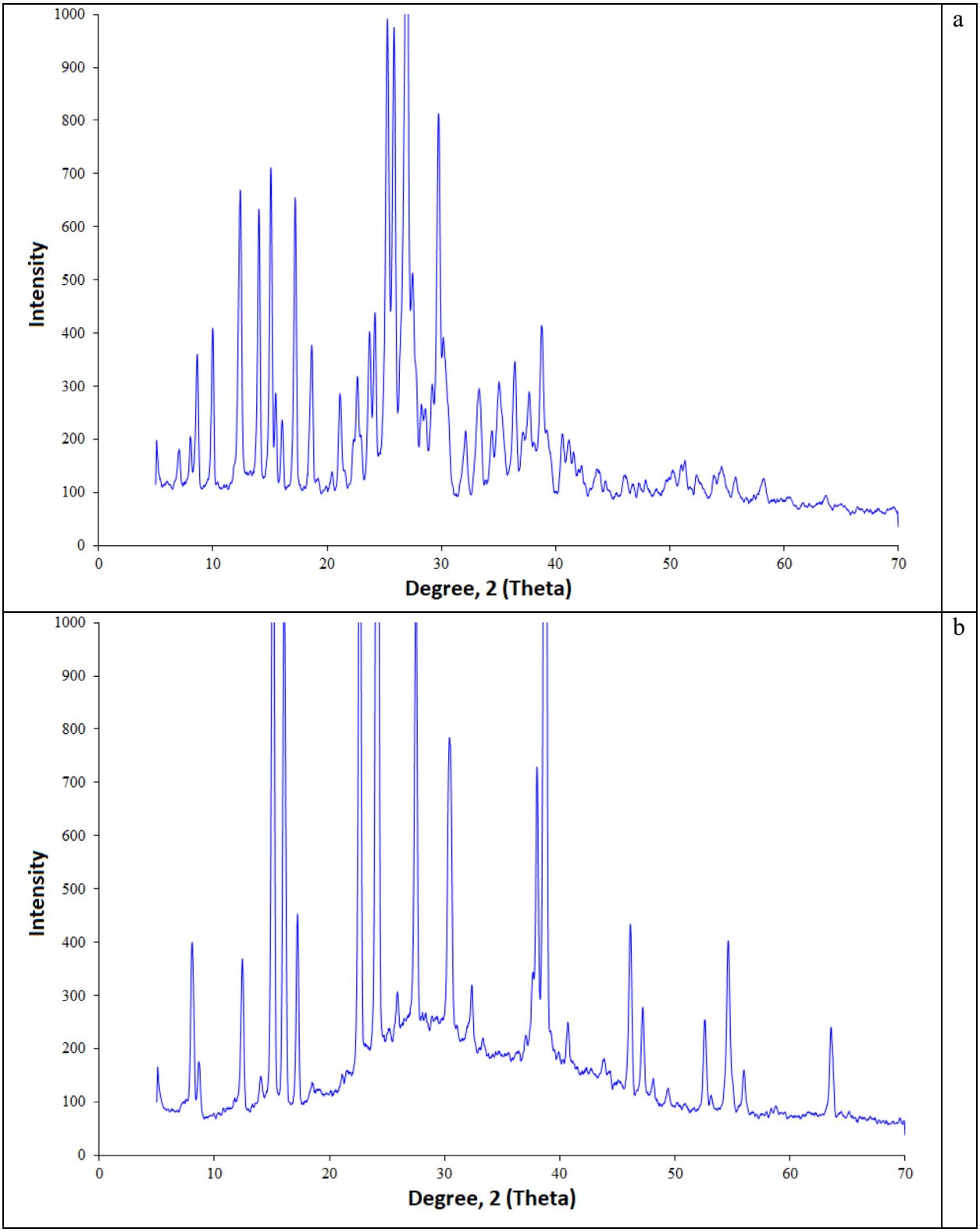

Fig. 2. XRD data: a - Biuret, b - Biuret water cluster.

3.3. NLO and thermodynamic properties of biuret-water clusters

NLO properties are important for frequency shift, optical modulation, switching, laser, fiber, optical material logic, and optical memory for emerging technologies in areas such as telecommunications, signal processing, and optical interface. compounds (Noureddine et al., 2021).

Non-linear optical properties (NLO), such as dipole moment, hyperpolarizability and polarizability for biuret-water clusters were calculated using the DFT method (Table 6). The effect on

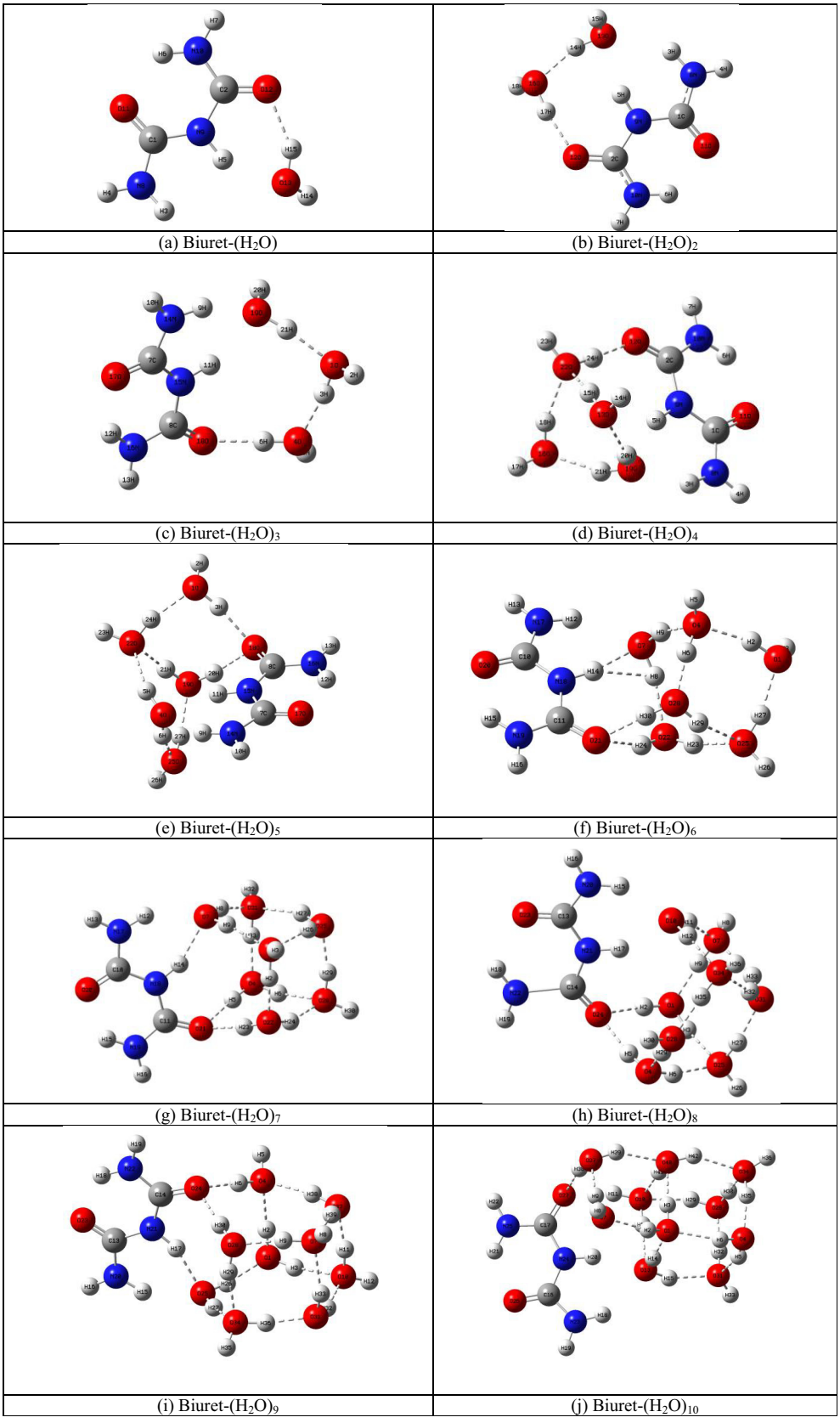

(a) Biuret-(H_2O) (b) Biuret-(H_2O)$_2$

(c) Biuret-(H_2O)$_3$ (d) Biuret-(H_2O)$_4$

(e) Biuret-(H_2O)$_5$ (f) Biuret-(H_2O)$_6$

(g) Biuret-(H_2O)$_7$ (h) Biuret-(H_2O)$_8$

(i) Biuret-(H_2O)$_9$ (j) Biuret-(H_2O)$_{10}$

Fig. 3. The Optimized structures of Biuret-water clusters.

Table 2
The structural parameters of Biuret-water clusters: Biuret-(H_2O), Biuret-$(H_2O)_2$, Biuret-$(H_2O)_3$, Biuret-$(H_2O)_4$, Biuret-$(H_2O)_5$.

Biuret-(H_2O)		**Biuret-$(H_2O)_2$**		**Biuret-$(H_2O)_3$**		**Biuret-$(H_2O)_4$**		**Biuret-$(H_2O)_5$**	
C1-N8	1.3701	C1-N8	1.3632	O1-H2	0.9613	C1-N8	1.3567	O1-H2	0.9644
C1-N9	1.389	C1-N9	1.3958	O1-H3	0.9868	C1-N9	1.4013	O1-H3	0.9859
C1-O11	1.2319	C1-O11	1.2327	O1-H21	1.716	C1-O11	1.2348	O1-H24	1.7355
*C*2-N9	1.4036	*C*2-N9	1.3934	H3-O4	1.7221	*C*2-N9	1.3857	H3-O18	1.7639
*C*2-O10	1.3476	*C*2-O10	1.3474	O4-H5	0.9612	*C*2-N10	1.3463	O4-H5	0.9757
*C*2-O12	1.2385	*C*2-O12	1.2425	O4-H6	0.9836	*C*2-O12	1.2475	O4-H6	0.9846
H3-N8	1.0091	H3-N8	1.0134	H6-O18	1.7445	H3-N8	1.0166	O5-H22	1.9572
H4-N8	1.0087	H4-N8	1.0077	C7-N14	1.3579	H4-N8	1.0071	H6-O25	1.7929
H5-N9	1.0217	H5-N9	1.0201	C7-N15	1.3997	H5-N9	1.0259	C7-N14	1.3558
H6-N10	1.0157	H6-N10	1.0165	C7-O17	1.2264	H6-N10	1.0175	C7-N15	1.4022
H7-N10	1.0074	H7-N10	1.0074	C8-N15	1.393	H7-N10	1.0071	C7-O17	1.2343
O12-H15	1.8677	O13-H14	0.9891	C8-N16	1.3465	O12-H24	1.6408	C8-N15	1.3801
O13-H14	0.9642	O13-H15	0.965	C8-O18	1.2348	O13-H14	0.9642	C8-N16	1.3429
O13-H15	0.9828	O12-H17	1.7547	H9-N14	1.014	O13-H15	0.9805	C8-O18	1.2554
		H14-O16	1.7497	*H*10-N14	1.0058	O13-H20	1.884	H9-N14	1.0157
		O16-H17	0.9893	*H*11-N15	1.0188	H15-O22	1.8528	*H*10-N14	1.0071
		O16-H18	0.964	H12-N16	1.0152	O16-H17	0.9643	*H*11-N15	1.0276
				H13-N16	1.0058	O16-H18	0.98	H12-N16	1.0182
				O19-H20	0.9621	O16-H21	1.8522	H13-N16	1.0074
				O19-H21	0.9883	H18-O22	1.8754	O18-H20	1.9672
						O19-H20	0.9793	O19-H20	0.9763
						O19-H21	0.981	O19-H21	0.9749
						O22-H23	0.9651	O19-H27	1.755
						O22-H24	1.001	H21-O22	1.9877
								O22-H23	0.9645
								O22-H24	0.9903
								O25-H26	0.9636
								O25-H27	0.9893

polarizability (α_0) of the water molecules numbers in biuret-water clusters is shown in Fig. 5.

According to the data shown in Table 6, the values of the dipole moment change nonlinearly with an increase in the number of molecules in aqueous biuret clusters. The maximum value (3.112 Debye) of the dipole moment is observed for the Biuret- $(H_2O)_4$ cluster, and the minimum value (1.212 Debye) is observed for the Biuret- $(H_2O)_7$ cluster. Hyperpolarisability values change in the same way. Maximum value ($12.771*10^{-31}$ e.s.u)Hyperpolarisability is observed for the Biuret- $(H_2O)_5$ cluster, and the minimum value ($6.139*10^{-31}$ e.s.u) - observed for the Biuret- (H_2O) cluster.

At the same time, the polarisability values increase almost linearly with an increase in the number of water molecules in aqueous biuret clusters with an R^2 value (0.9948). A similar phenomenon was observed in the case of thiourea (Akman et al., 2020) and ammonium sulfamate (Kazachenko et al., 2021).

Various thermodynamic functions are used to predict the reactivity of chemicals and to determine the likelihood of different reaction routes (Fazilath Basha et al., 2021).Standard thermodynamic functions such as zero-point energy correction, heat capacity, entropy (S) electronic energy (EE), thermal correction to energy, thermal correction to enthalpy, thermal correction to free energy, and other parameters were calculated using B3LYP methods with a basis set of 6–31 + G (d, p) (Table 7).

According to the data given in Table 7 and Fig. 6, the values of E (Thermal), Heat Capacity (Cv), Entropy (S) increase linearly as water molecules in the biuret cluster increase. For the change in E (Thermal) R^2 = 1, which is high. For the dependence of the change in Heat Capacity (Cv) on the content of water molecules in the water cluster of biuret, R^2 = 0.9939 is observed. For the dependence of the change in Entropy (S) on the content of water molecules in the aqueous biuret cluster, R^2 = 0.9325 is observed.

It should be noted that other thermodynamic characteristics also change almost linearly with a regular change in water molecules in the biuret cluster. A similar phenomenon was also observed in (Kazachenko et al., 2021).

3.4. HOMO-LUMO analysis and electronic parameters of Biuret-$(H_2O)_n$ clusters

Frontier molecular orbitals (FMO) are a valuable practical model for describing chemical reactivity. This theory permit the identification of electrophilic and nucleophilic attacks which responsible to the formation of hydrogen bonding interactions. An important aspect of the theory of boundary electrons is the emphasis on the busiest and lowest unoccupied molecular orbitals (HOMO and LUMO). So, according to this theory, attention is paid to the localization of the HOMO orbital, because electrons from this orbital are most free to participate in the reaction. Likewise, the boundary orbit theory predicts that the location of the lowest unoccupied orbital (LUMO) is a good electrophilic site (Gatfaoui et al., 2019).

Using the energy gap between HOMO-LUMO, ionization potential (IP), electronegativity (χ), softness(ς),electron affinity (EA), electrophilicity index (ω),chemical potential (μ) (Table 8) were calculated (at B3LYP/6–31 + G(d,p) basis set, according (Fleming, 1976) by the following equations:

$$IP = -E_{HOMO} \tag{2}$$

$$EA = -E_{LUMO} \tag{3}$$

$$\chi = -1/2(E_{LUMO} + E_{HOMO}) \tag{4}$$

$$\mu = 1/2(E_{LUMO} + E_{HOMO}) \tag{4}$$

$$\eta = 1/2(E_{LUMO} - E_{HOMO}) \tag{5}$$

$$\zeta = \frac{1}{\eta} \tag{5}$$

$$\omega = \frac{\mu^2}{2\eta} \tag{6}$$

Table 3
The structural parameters of Biuret-water clusters: Biuret-$(H_2O)_6$, Biuret-$(H_2O)_7$, Biuret-$(H_2O)_8$, Biuret-$(H_2O)_9$, Biuret-$(H_2O)_{10}$.

Biuret-$(H_2O)_6$		**Biuret-$(H_2O)_7$**		**Biuret-$(H_2O)_8$**		**Biuret-$(H_2O)_9$**		**Biuret-$(H_2O)_{10}$**	
O1-H2	0.9853	O1-H2	1.0029	O1-H2	0.979	O1-H2	0.9755	O1-H2	0.9853
O1-H3	0.9648	O1-H3	0.9648	O1-H3	0.9784	O1-H3	0.9773	O1-H3	0.9874
O1-H27	1.7327	O1-H9	1.8579	O1-H9	1.6438	O1-H26	1.7459	O1-H6	1.9219
H2-O4	1.7939	O1-H26	1.9227	H2-H24	1.8715	H2-O4	1.9493	O1-H14	1.7329
O4-H5	0.9651	H2-H22	1.6563	H3-H25	1.8994	H3-O10	1.9145	H2-O7	1.8013
O4-H6	1.0059	O4-H5	0.9787	O4-H5	0.977	O4-H5	0.9653	H3-O40	1.7952
O4-H9	1.9351	O4-H6	0.9779	O4-H6	0.9789	O4-H6	0.9891	O4-H5	0.9764
H6-O28	1.6406	O4-H33	1.6563	O4-H29	1.6593	O4-H38	1.8858	O4-H6	0.9781
O7-H8	0.9862	H5-O21	1.8863	H5-O24	1.8893	H6-O24	1.7409	O4-H35	1.6905
O7-H9	0.9763	H6-O28	1.9058	H6-O25	1.8707	O7-H8	0.9647	H5-O31	1.9595
O7-H14	1.8288	O7-H8	0.9802	O7-H8	0.9647	O7-H9	1.0018	O7-H8	0.9639
H8-H14	2.0819	O7-H9	0.9802	O7-H9	1.0045	O7-H33	1.9216	O7-H9	0.9898
H8-O22	1.8322	O7-H14	1.8744	O7-*H*11	1.8428	O7-H39	1.8559	H9-O37	1.7538
C10-N17	1.361	H8-O31	1.8579	O7-H33	1.9138	H9-O28	1.6533	O10-*H*11	0.98
C10-N18	1.3973	C10-N17	1.3572	O10-*H*11	0.9805	O10-*H*11	1.0019	O10-H12	0.9807
C10-O20	1.2333	C10-N18	1.4011	O10-H12	0.9798	O10-H12	0.9649	O10-H29	1.999
C11-N18	1.3845	C10-O20	1.2341	H12-O34	1.853	O10-H32	1.8747	O10-H41	1.7914
C11-N19	1.3447	C11-N18	1.3836	C13-N20	1.3563	*H*11-O37	1.6594	*H*11-O27	1.9157
C11-O21	1.2504	C11-N19	1.3435	C13-N21	1.4021	C13-N20	1.3548	H12-O13	1.8985
H12-N17	1.0143	C11-O21	1.2518	C13-O23	1.2346	C13-N21	1.404	O13-H14	0.9946
H13-N17	1.0075	H12-N17	1.0158	C14-N21	1.385	C13-O23	1.2346	O13-H15	0.9814
H14-N18	1.0285	H13-N17	1.0072	C14-N22	1.3441	C14-N21	1.3765	H15-O31	1.8648
H15-N19	1.0173	H14-N18	1.0271	C14-O24	1.2505	C14-N22	1.3425	C16-N23	1.359
H16-N19	1.0075	H15-N19	1.0177	H15-N20	1.0171	C14-O24	1.2583	C16-N24	1.4007
O21-H24	2.0134	H16 -N19	1.0075	H16-N20	1.0072	H15-N20	1.0174	C16-O26	1.232
O21-H30	1.8644	O21-H23	1.8863	H17-N21	1.0256	H16-N20	1.0072	C17-N24	1.388
O22-H23	0.9753	O22-H23	0.9787	H18-N22	1.0179	H17-N21	1.0329	C17-N25	1.343
O22-H24	0.9756	O22-H24	0.9779	H19-N22	1.0076	H17-O25	1.8091	C17-O27	1.2499
H23-O25	1.9372	H24-O28	1.9061	O25-H26	0.9647	H18-N22	1.0185	H18-N23	1.0146
O25-H26	0.9647	O25-H26	0.9779	O25-H27	1.0003	H19-N22	1.0075	H19-N23	1.0076
O25-H27	0.9907	O25-H27	0.9779	H27-O31	1.6716	O24-H30	1.8866	H20-N24	1.0175
O25-H29	1.9415	O25-H29	1.6852	O28-H29	0.9998	O25-H26	0.9903	H21-N25	1.0174
O28-H29	0.9768	H27-O31	1.9219	O28-H30	0.9637	O25-H27	0.9792	H22-N25	1.0076
O28-H30	0.9799	O28-H29	0.9993	O28-H35	1.647	H27-O34	1.8597	O27-H38	1.9624
		O28-H30	0.9645	O31-H32	0.979	O28-H29	0.9791	O28-H29	0.9744
		O31-H32	0.9648	O31-H33	0.9777	O28-H30	0.9777	O28-H30	0.9795
		O31-H33	1.0029	H32-O34	1.8825	H29-O34	1.8917	O28-H32	1.6752
				O34-H35	1.0004	O31-H32	0.9799	H30-O34	1.9012
				O34-H36	0.9649	O31-H33	0.9779	O31-H32	1.0007
						O31-H36	1.6489	O31-H33	0.965
						O34-H35	0.9651	O34-H35	0.9992
						O34-H36	1.0033	O34-H36	0.9649
						O37-H38	0.978	O34-H42	1.9657
						O37-H39	0.9799	O37-H38	0.9757
								H39-O40	2.0021
								O40-H41	0.9855
								O40-H42	0.9761

A small band gap indicates that the molecule has high polarization, chemical reactivity and biological activity, and low kinetic stability (Bader, 1990). Based on the lower energy gap, it should be noted that the biuret cluster with nine water molecules has a higher chemical stability than other clusters.

According to the data presented in Table 8, the Softness values practically do not change with an increase in the number of water molecules in the biuret cluster and are 0.13–0.14. The Electronegativity values change nonlinearly with an increase in the number of water molecules in the biuret cluster, while the minimum Electronegativity (25.67) corresponds to the minimum number of water molecules in the biuret cluster, and the maximum Electronegativity (32.79) corresponds to the maximum number of water molecules (in the us spaces (1–10)). Electrophilicity values also change non-linearly. The minimum Electrophilicity value (3.83) corresponds to the Biuret- (H_2O) cluster, and the maximum Electrophilicity value (4.295) corresponds to the Biuret- $(H_2O)_9$ cluster. Other characteristics, such as Ionisation energy, Electron affinity, Chemical potential and Chemical hardness, change nonlinearly with an increase in the amount of water in the water clusters of biuret.

3.5. AIM, RDG and ELF topological analysis

The theory of atoms in molecules (AIM) is actively used to determine the types of interactions in various molecular systems (Johnson et al., 2010). Topological parameters such as electron density ρ (r), the Laplacian of electron density $\nabla^2\rho$ (r), potential energy density V (r), Lagrangian kinetic energy G (r), Kinetic energy of Hamiltonian H (r) = G (r) + V (r) and the binding energy E_{int} = V (r) / 2 can help to understand the properties of hydrogen bonds between compounds (Akman et al., 2020). The Molecular diagram of the Biuret-water clusters is shown in Fig. 7.

According to (Johnson et al., 2010), the interactions of hydrogen bonds can be defined as follows:

(1) $\nabla^2\rho$ (r) > 0 and H (r) > 0 = Weak hydrogen bonds;
(2) $\nabla^2\rho$ (r) > 0 and H (r) < 0 = Moderate hydrogen bonds;
(3) $\nabla^2\rho$ (r) < 0 and H (r) < 0 = Strong hydrogen bonds.

The electron density ρ (r) and its Laplacian $\nabla^2\rho$(r) help determine the nature of interactions. On the whole, large values of the electron density ρ (r) and its Laplacian $\nabla^2\rho$(r) show the power of

Table 4
Hydrogen bonding interactions parameters of Biuret-water clusters.

	H-Bond	X-H…X	X…X
Biuret-(H2O)	O13-H15…O12	1.867	2.75
Biuret-(H2O)2	O16- H17…O12	1.75	2.73
	O13-H14…O16	1.74	2.69
Biuret-(H2O)3	O4-H14…O16	1.74	2.72
	O1-H3…O4	1.72	2.70
	O19-H21…O1	1.71	2.69
Biuret-(H2O)4	O22-H24…O12	1.64	2.64
	O16-H18…O22	1.87	2.82
	O19-H21…O16	1.85	2.78
	O13-H15…O22	1.85	2.79
	O19-H20…O13	1.88	2.08
Biuret-(H2O)5	O1-H3…O18	1.76	2.74
	O19-H20…O18	1.96	2.91
	O22-H24…O1	1.73	2.69
	O4-H5…O22	1.95	2.88
	O4-H6…O25	1.79	2.74
	O25-H27…O19	1.75	2.71
Biuret-(H2O)6	N18-H14…O7	1.82	2.83
	N18-H14…O8	2.01	3.04
	O7-H9…O4	1.93	2.87
	O1-H2…O4	1.79	2.75
	O25-H27…O1	1.73	2.70
	O28-H29…O25	1.94	2.86
	O22-H23…O25	1.93	2.87
	O4-H6…O28	1.64	2.63
	O28-H30…O21	1.86	2.83
	O22-H24…O21	2.01	2.95
	O7-H8…O22	1.83	2.77
Biuret-(H2O)7	N18-H14…O7	1.87	2.85
	O7-H8…O31	1.85	2.80
	O25-H27…O31	1.92	2.85
	O4-H5…O21	1.88	2.85
	O22-H23…O21	1.88	2.85
	O31-H33…O4	1.65	2.65
	O4-H6…O28	1.90	2.83
	O22-H24…O28	1.96	2.83
	O28-H29…O25	1.68	2.66
	O25-H27…O31	1.92	2.85
	O25-H26…O1	1.92	2.85
	O1-H2…O22	1.65	2.65
Biuret-(H2O)8	O1-H2…O24	1.87	2.83
	O4-H5…O24	1.88	2.85
	O4-H6…O25	1.87	2.83
	O25-H27…O31	1.67	2.66
	O31-H32…O34	1.88	2.84
	O10-*H*11…O7	1.84	2.79
	O31-H33…O7	1.91	2.84
	O10-H12…O34	1.85	2.82
	O7-H9…O1	1.64	2.63
	O1-H3…O25	1.89	2.83
	O34-H35…O28	1.64	2.64
	O28-H29…O4	1.65	2.65
Biuret-(H2O)9	O4-H6…O24	1.74	2.72
	O1-H2…O4	1.94	2.90
	O28-H30…O24	1.88	2.86
	N21-H17…O25	1.80	2.79
	O25-H27…O34	1.85	2.82
	O28-H29…O34	1.89	2.84
	O7-H9…O28	1.65	2.64
	O34-H36…O31	1.64	2.64
	O1-H3…O10	1.91	2.86
	O31-H32…O10	1.87	2.82
	O10-*H*11…O37	1.65	2.64
	O37-H38…O4	1.88	2.84
	O37-H39…O7	1.85	2.81
	O25-H26…O1	1.74	2.72
Biuret-(H2O)10	O37-H38…O27	1.96	2.92
	O37-H39…O40	2.00	2.89
	O7-H9…O37	1.75	2.72
	O1-H2…O7	1.80	2.73
	O1-H3…O40	1.79	2.77
	O13-H14…O1	1.73	2.71
	O28-H29…O10	1.99	2.86
	O28-H30…O34	1.90	2.84
	O40-H42…O34	1.96	2.84
	O34-H35…O4	1.69	2.67
	O4-H5…O31	1.95	2.88
	O13-H15…O31	1.86	2.80
	O31-H32…O28	1.67	2.66
	O10-H12…O13	1.89	2.87
	O4-H6…O1	1.92	2.82

Table 5
Energy values of Biuret-water clusters computed at B3LYP/6–31 + G(d,p) level of theory.

Number of water molecules	Energy (kJ/mol)	Bonding energy ΔE (kJ/mol)
1	−1235219	−58.45
2	−1435939	−111.45
3	−1637131	−636.45
4	−1837404	−242.45
5	−2038123	−294.45
6	−2238843	−347.45
7	−2439589	−426.45
8	−2640308	−478.45
9	−2841053	−556.45
10	−3041747	−583.45

hydrogen interactions. Negative values of the Laplacian $\nabla^2\rho(r)$ indicate a strong covalent character, while positive values indicate a decrease in the charge in the internuclear region (Akman et al., 2020; Kazachenko et al., 2021).

In the Biuret-(H_2O) cluster, three types of interactions were observed: O13-H15…O12, N9-H5…O13, N10-H6…O11, where the electron density values are 0.0312, 0.0256, 0.0290a. u. and the Laplacian values are 0.0887, 0.0775, 0.0912a. u. respectively. As clearly seen from Table 9, the first hydrogen bond (O13-H15…O12) was matched to the biggest binding energy with value equal to 62.16 kcal/mol. In the Biuret-$(H_2O)_2$ cluster, five H-bonds interactions were observed: N8-H3…O13, N9-H6…O13, O16-H17…O12, O13-H14…O16, N10-H6…O11, where the electron density values are 0.0139, 0.0267, 0.0380, 0.0390, 0.0288a. u. and the Laplacian values are 0.0445, 0.0742, 0.1122, 0.1171, 0.0898a. u. respectively. The major interaction energy value corresponds to the fourth hydrogen bond with 76.85 kcal/mol. In the Biuret-$(H_2O)_3$ cluster, three types of interactions were observed: N14-H9…O19, N15-*H*11…O19, N16-H12…O17, O19-H21…O1, O1-H3…O4, O4-H6…O18, where the electron density values are 0.0211, 0.0226, 0.0290, 0.0421, 0.0411, 0.0367a. u. and the Laplacian values are 0.0807, 0.0792, 0.1103, 0.1347, 0.1347, 0.1308a. u. respectively. In the Biuret-$(H_2O)_4$ cluster, three types of interactions were observed: N18-H3…O19, O19-H20…O13, N9-H5…O19, O19-H21…O16, O13-H15…O22, O22-H24…O12, N10-H6…O11, where the electron density values are 0.0216, 0.0289, 0.0300, 0.0313, 0.0308, 0.0487, 0.0308a. u. and the Laplacian values are 0.0654, 0.0847, 0.0822, 0.0913, 0.0903, 0.1459, 0.0960a. u. respectively. Concerning Biuret-$(H_2O)_5$ cluster, three types of interactions were observed: N16-H12…O17, N15-*H*11…O4, N14-H9…O4, O4-H5…O22, O25-H27…O19, O1-H3…O18, O19-H20…O18, O22-H24…O1, O4-H6…O25, where the electron density values are 0.0307, 0.0321, 0.0195, 0.2451, 0.0398, 0.0361, 0.0232, 0.0402, 0.0349a. u. and the Laplacian values are 0.0956, 0.0857, 0.0597, 0.0710, 0.1139, 0.1113, 0.0677, 0.1195, 0.1053a. u. respectively. The $E_{H\ldots O}$ energy value of these interactions were ranging from 40 to 77 kcal/mol. Regarding Biuret-$(H_2O)_6$ cluster, three types of interactions were observed: N17-H12…O7, N18-H14…O7, O28-H30…O21, O22-H24…O21, O1-H2…O4, O4-

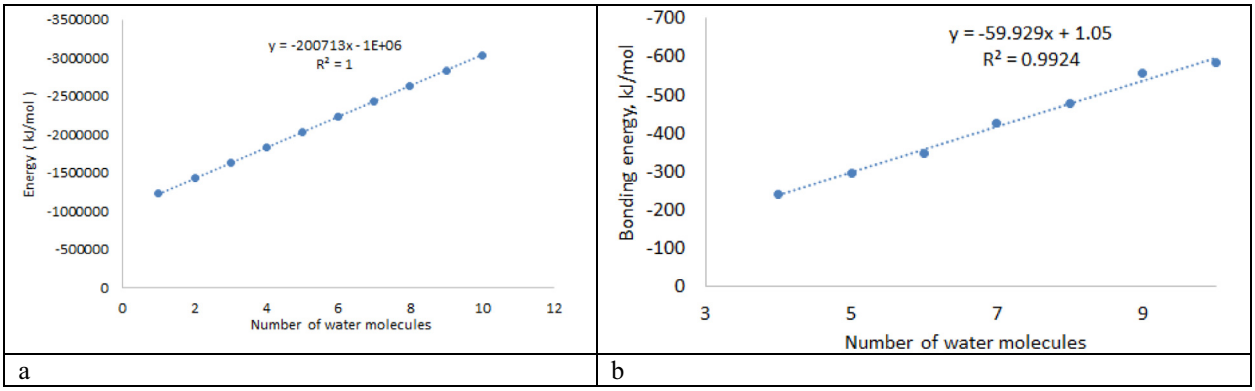

Fig. 4. Influence of the number of water molecules in water clusters on: (a) - Energy, (б) - Bonding energy.

H6…O28, O25-H27…O1, O7-H8…O22, O7-H9…O4, O28-H29…O25, O22-H23…O25, O22-H23…O21, where the electron density values are 0.0140, 0.0358, 0.0284, 0.0220, 0.0355, 0.0523, 0.0408, 0.0337, 0.0259, 0.0256, 0.0254, 0.0220a. u. and the Laplacian values are0.0447, 0.0693, 0.0864, 0.0608, 0.0141, 0.1407, 0.1197, 0.0941, 0.0472, 0.0736, 0.0740, 0.0608a. u. respectively. In the Biuret-$(H_2O)_7$ cluster, twelve hydrogen bonding interactions were identified: N17-H12…O7, N18-H14…O7, N19-H15…O20, O4-H5…O21, O22-H23…O21, O31-H33…O4, O4-H6…O28, O22-H24…O28, O25-H27…O31, O1-H2…O22, O25-H26…O1, O7-H9…O1,where the electron density values are 0.0200, 0.0322, 0.0302, 0.0272, 0.0272, 0.0501, 0.0275, 0.0275, 0.0269, 0.0501, 0.0268, 0.0306a. u. and the Laplacian values are0.0607, 0.0877, 0.0940, 0.0817, 0.0818, 0.1372, 0.0800, 0.0799, 0.0768, 0.1372, 0.0767, 0.0893a. u. respectively. In the Biuret-$(H_2O)_8$ cluster, three types of interactions were observed: N20-H15…O10, N21-H17…O10, N22-H18…O23, O1-H2…O24, O4-H5…O24, O10-H12…O34, O10-*H*11…O7, O31-H32…O34, O31-H33…O7, O25-H27…O31, O1-H3…O25, O4-H6…O25, O34-H35…O28, O28-H29…O4, O7-H9…O1,where the electron density values are0.0228, 0.0290, 0.0309, 0.0279, 0.0263, 0.0305, 0.0315, 0.0292, 0.0273, 0.0483, 0.0280, 0.0296, 0.0494, 0.0492, 0.0518a. u. and the Laplacian values are0.0688, 0.0786, 0.0963, 0.0853, 0.0816, 0.0897, 0.0928, 0.0830, 0.0782, 0.1337, 0.0810, 0.0863, 0.1429, 0.1378, 0.1404a. u. respectively. In the Biuret-$(H_2O)_9$ cluster, three types of interactions were observed: N20-H15…O25, N21-H17…O25, N22-H18…O23, O4-H6…O24, O28-H30…O24, O28-H29…O34, O25-H27…O34, O37-H38…O4, O1-H3…O10, O10-*H*11…O37, O31-H32…O10, O31-H33…O7, O37-H39…O7, O7-H9…O28, O34-H36…O31, O25-H26…O1,where the electron density values are 0.0214, 0.0372, 0.0309, 0.0379, 0.0273, 0.0285, 0.0303, 0.0286, 0.0272, 0.0502, 0.0296, 0.0268, 0.0306, 0.0502, 0.0511, 0.0402a. u. and the Laplacian values are 0.0641, 0.1023, 0.0959, 0.1168, 0.0809, 0.0812, 0.0887, 0.0829, 0.0774, 0.1374, 0.0851, 0.0765, 0.0899, 0.1394, 0.1396, 0.1153a. u. respectively.In the Biuret-$(H_2O)_{10}$ cluster, three types of interactions were observed: N25-H21…O26, N24-H20…O13, N23-H18…O13, O10-*H*11…O27, O37-H38…O27, O37-H39…O40, O40-H42…O34, O4-H6…O1, O28-H29…O10, O13-H15…O31, O4-H5…O31, O28-H30…O34, O40-H41…O10, O13-H14…O1, O1-H2…O7, O7-H9…O37, O34-H35…O4,where the electron density values are 0.0294, 0.0243, 0.0157, 0.0229, 0.0270, 0.0213, 0.0246, 0.0261, 0.0216, 0.0302, 0.0248, 0.3371, 0.0372, 0.0423, 0.0347, 0.0394, 0.0464a. u. and the Laplacian values are 0.0917, 0.0718, 0.0455, 0.0675, 0.0779, 0.0658, 0.0717, 0.00786, 0.0679, 0.0879, 0.0700, 1.8245, 0.1045, 0.1175, 0.1032, 0.1133, 0.1282a. u. respectively. As it is shown in Table 9, the O28-H30…O34 bond was associated to the bigger interaction energy which is in the range 1449.22 kcal/mol.

The Reduced Density Gradient (RDG) function is used to understand non-covalent interactions as a wide range of real space in a molecule. Its value is determined by the electron density ρ (r) and the first derivative (Contreras Aguilar et al., 2019):

$$RDG(r) = \frac{1}{2(3\pi^2)^{1/3}} \frac{|\nabla\rho(r)|}{\rho(r)^{4/3}} \quad (7)$$

The peaks of the two-dimensional plots of the dependence of the reduced gradient on the sign of (λ_2) ρ, that is, non-covalent interactions appear in areas of low density and low gradient. The sign of the second sign of the Hessein eigenvalue (λ_2) is introduced to distinguish between different types of non-covalent interactions, and the density ρ represents the strength of interactions

Table 6
The Dipole moment (Debye), polarizability (10^{-24} e.s.u) and hyperpolarizability (10^{-31} e.s.u) of Biuret-water clusters.

Number of water molecule	Dipole moment	Polarisability	Hyperpolarisability
1	1.758	9.429	6.139
2	2.068	10.080	7.460
3	1.796	12.376	9.667
4	3.112	13.614	9.609
5	2.896	14.664	12.771
6	2.500	15.931	8.501
7	1.212	17.281	10.868
8	2.215	19.004	10.405
9	1.567	20.659	6.170
10	2.031	21.462	7.787

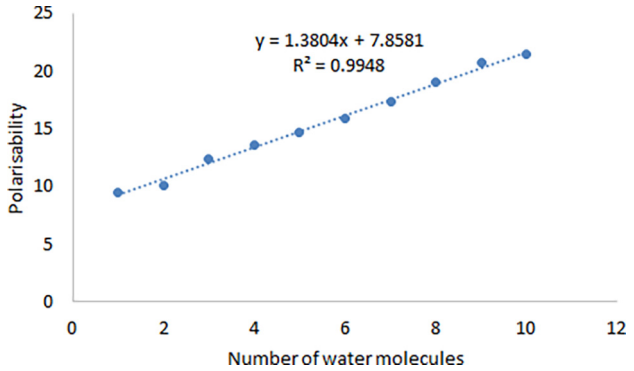

Fig. 5. The effect on polarizability of the number of water molecules in biuret-water clusters.

Table 7
The thermodynamic parameters calculated at 298.15 K for the different Biuret-water clusters using B3LYP/6–31 + G(d,p).

Parameters	1	2	3	4	5	6	7	8	9	10
E(RB3LYP)	−470.4703	−546.9272	−623.5516	−699.8305	−776.2813	−852.7348	−929.1959	−1005.6473	−1082.1018	−1158.5479
Electronic Energy (EE)	−470.4703	−546.9272	−623.5516	−699.8305	−766.2818	−852.7348	−929.1959	1005.6473	−1082.1018	−1158.5479
Zero-point Energy Correction	0.1159	0.1418	0.1664	0.19301	0.2187	0.2455	0.2722	0.2972	0.3237	0.3503
Thermal Correction to Energy	0.1260	0.1543	0.1819	0.2106	0.2388	0.2676	0.2960	0.3238	0.3532	0.3814
Thermal Correction to Enthalpy	0.1270	0.1553	0.1829	0.2116	0.2398	0.2685	0.2970	0.3247	0.3532	0.3823
Thermal Correction to Free Energy	0.0807	0.1031	0.1231	0.1474	0.1701	0.1948	0.2200	0.2412	0.2656	0.2890
EE + Zero-point Energy	−470.3544	−546.7854	−623.3851	−699.6374	−776.0638	−852.4892	−928.9237	−1005.3499	−1081.7780	−1158.1976
EE + Thermal Energy Correction	−470.3442	−546.7728	−623.3697	−699.6198	−766.0429	−852.4671	−928.8999	−1005.3234	−1081.7494	−1158.1665
EE + Thermal Enthalpy Correction	−470.3433	−546.7719	−623.3687	−699.6188	−766.0419	−852.4662	−928.9888	−1005.3225	−1081.7485	−1158.1655
EE + Thermal Free Energy Correction	−470.3896	−546.8241	−623.4285	−699.6830	−766.1117	−852.5399	−928.9758	−1005.4060	−108.8361	−1158.2588
E (Thermal)	79.12	96.881	114.186	132.201	149.91	167.933	185.779	203.209	221.080	239.348
Heat Capacity (Cv)	35.33	43.661	52.922	61.305	69.603	76.988	84.144	72.880	100.659	109.245
Entropy (S)	97.39	109.75	125.876	135.098	146.736	155.039	161.861	175.904	184.415	196.433

Fig. 6. The variation of thermodynamic parameters as a function of the water molecules numbers in the biuret-water clusters.

(Becke and Edgecombe, 1990). The force interactions in the molecular system, which indicate a stronger attractiveness of blue and a push of red, is analyzed using Multiwfn and VMD software.

The RDG scatter graphs of Biuret-$(H_2O)_{(1-10)}$ clusters were indicated in Fig. 8. Based on the color scale of RDG and VMD visual representation, we can identify each type of interaction. The red, the green and the blue colors were respectively matched to steric effect, van der Waals interaction and hydrogen bonding contact. As clearly seen from RDG graphs, the hydrogen interactions appear in the range (-0.05)-(-0.02) a.u. The van der Waals interaction ranging from −0.02 to 0.01 a.u. While to range between 0.01 and 0.05 a.u was concerned to ring steric effect.

Important methods for studying the electronic structure of molecules free from an arbitrary choice of molecular orbitals are topological analysis of the electron density by Bader (AIM) (Johnson et al., 2010) and topological analysis of ELF (Michalski et al., 2019). The electronic structure of a molecule described by ELF is represented by maxima (attractors) and its field localization region η (r), which characterize covalent bonds, lone pairs, nuclear regions, and valence shells in atoms (Fuster et al., 2000).

The spatial position of these attractors makes it possible to differentiate the core basins and the valence basins (Kazachenko et al., 2021). Heart basins are located around nuclei (except for the hydrogen atom). The valence basins are classified according to their connectivity with the core basins. Topological analysis of the localization function of electrons constitutes the suitable mathematical model for the characterization of chemical bonds. The electron density, ELF diagrams of the different biuret-water clusters are shown in Fig. 9. The ELF color code range between blue and red, as shown in Fig. 9. The minimum Pauli repulsion correspond to blue regions. While the areas with maximum Pauli repulsion were colored by the red. In addition, the charge delocalization regions with ELF < 0.5 were mapped as blue spots. Whereas, the red electron localization areas with ELF > 0.5 were associated to covalent bonds.

3.6. Electrostatic potential (ESP) analysis of Biuret-water clusters

Calculation of the electronic characteristics of various materials is important for understanding their functionality and reactivity (Timmer and Mooibroek, 2021).

Electrostatic potential (ESP) or molecular electrostatic potential (MEP) has been actively used in scientific research for several decades (Sharma and Tiwari, 2016). Surface analysis by electrostatic potential (ESP) is one of the factors that can play an important role in the design of various substances (Drissi et al., 2015). Molecular

Table 8
The electronic parameters of the different Biuret-water clusters.

	E_{HOMO}	E_{LUMO}	Gap	Ionisation energy	Electron affinity	Chemical potential	Chemical hardness (η)	Softness	Electronegativity	Electrophilicity
1	−7,33	−0,33	−7	7,33	0,33	−3,83	3,5	0,14	25,67	3,83
2	−7,76	−0,16	−7,6	7,76	0,16	−3,96	3,8	0,13	29,79	3,96
3	−7,76	−0,66	−7,1	7,76	0,66	−4,21	3,55	0,14	31,46	4,21
4	−7,58	−0,19	−7,39	7,58	0,19	−3,88	3,695	0,13	27,88	3,885
5	−7,68	−0,27	−7,41	7,68	0,27	−3,97	3,705	0,13	29,27	3,975
6	−7,75	−0,3	−7,45	7,75	0,3	−4,02	3,725	0,13	30,17	4,025
7	−7,76	−0,3	−7,46	7,76	0,3	−4,03	3,73	0,13	30,28	4,03
8	−7,73	−0,32	−7,41	7,73	0,32	−4,02	3,705	0,13	30,01	4,025
9	−7,77	−0,82	−6,95	7,77	0,82	−4,29	3,475	0,14	32,05	4,295
10	−7,93	−0,44	−7,49	7,93	0,44	−4,18	3,745	0,13	32,79	4,185

electrostatic potential is the potential that a single positive charge will experience at any point surrounding a molecule, due to the distribution of electron density in the molecule. Electrostatic potential is considered to be a predictor of chemical reactivity, since areas of negative potential are expected to be sites of protonation and nucleophilic attack, while areas of positive potential may indicate electrophilic sites [50].

Different electrostatic potential values are indicated by different colors in the ESP (Fig. 10). A decreasing order potential is expressed as follows: blue > green > yellow > orange > red. Negative values are shown in red and are associated with the area of electrophilic attack and mainly with oxygen atoms in biuret, water, and the biuret-water cluster. The nucleophilic attack area (positive area) is shown in blue and is mainly associated with the hydrogen and nitrogen atoms in the biuret and the biuret-water cluster. As clearly seen from Fig. 10, the oxygen atoms of biuret-water cluster were colored with red color (nucleophilic sites). Whereas, the electrophilic sites were localized on hydrogen atoms (blue color).

4. Conclusions

In this work, water clusters of biuret (n = 1–10) were investigated by FTIR, XRD, AIM, DFT, RDG, ELF, NLO methods. It is shown that the introduction of water molecules into the biuret cluster leads to an increase in the intensity of the FTIR spectra. The inclusion of water molecules in a biuret crystal leads to a significant increase in the intensity of most peaks in the range from 14 to 65 2⊖ (deg). All calculations of biuret clusters - (H_2O) (1–10) were carried out in the gas phase at the level of the B3LYP / 6–31 + G (d, p) theory. The strength of hydrogen bond interactions is discussed using the AIM topological analysis. We also studied the NLO properties for each cluster using the RB3LYP functionality. It was shown that the values of E (Thermal), Heat Capacity (Cv), Entropy (S) increase linearly with an increase in water molecules in the biuret cluster.

Declarations

Compliance with ethical standards.

5. Ethics approval

N/A. In the course of work on this article, the authors did not conduct research on animals and humans in any form.

Declaration of Competing Interest

The authors declare that they have no known competing financial interests or personal relationships that could have appeared to influence the work reported in this paper.

Acknowledgments

Experimental work was conducted within the framework of the budget plan # 0287-2021-0017 for Institute of Chemistry and Chemical Technology SB RAS using the equipment of Krasnoyarsk Regional Research Equipment Center of SB RAS. Theoretical work was supported Researchers Supporting Project number (RSP - 2021/61), King Saud University, Riyadh, Saudi Arabia. The authors are grateful to G.N. Bondarenko for the X-ray study and E.V. Elsuf'ev for recording the FTIR spectra.

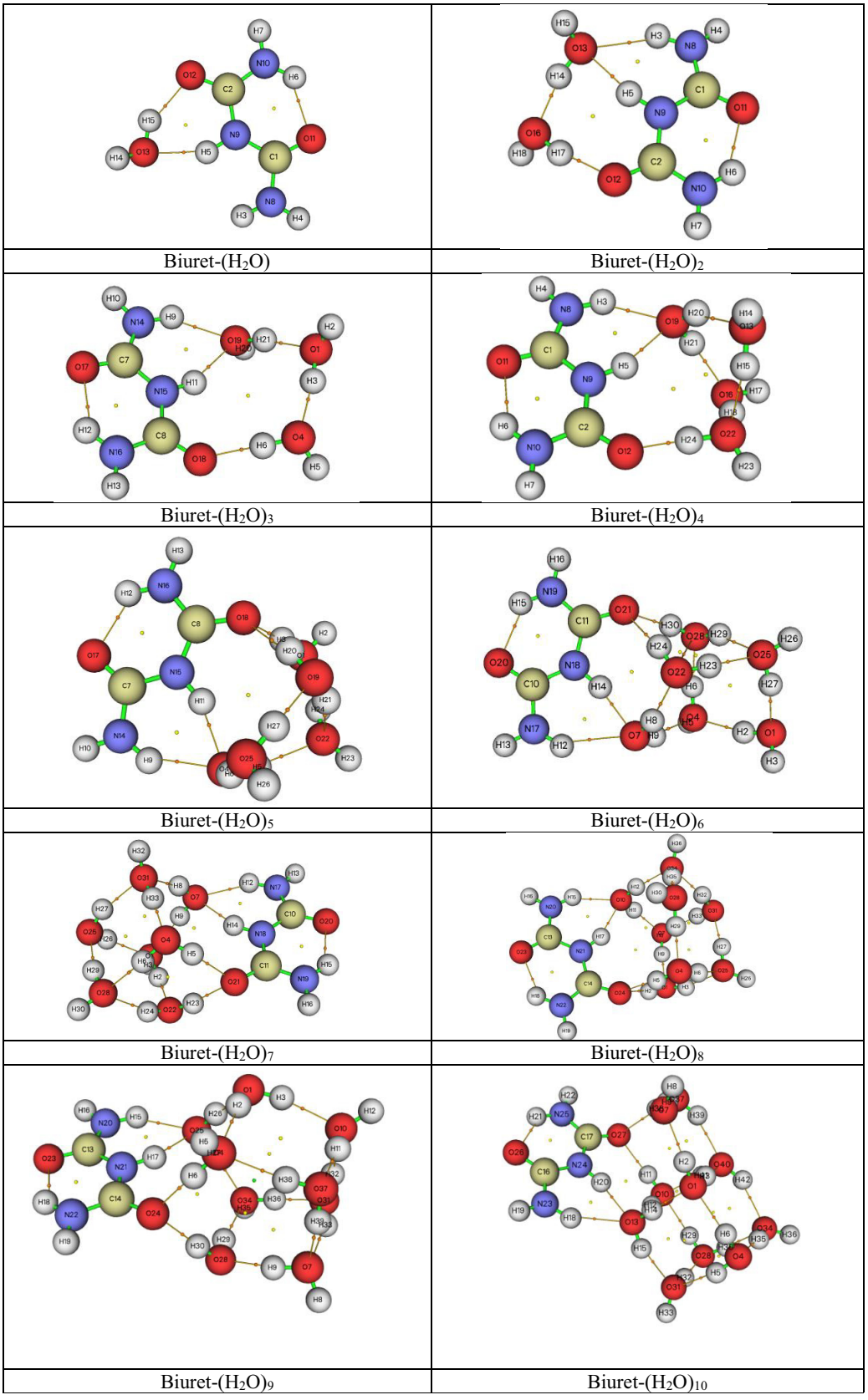

Fig. 7. AIM graphical visualization of Biuret-water clusters.

Table 9
The topological parameters of H-bond interactions at BCP calculated for the various clusters.

	H-bonds	ρ	Δρ	H	V_{BCP}	$E_{H\ldots O}$
1	O13-H15…O12	0.0312	0.0887	−0.7661 0.10^{-3}	−0.0237	62.16
	N9-H5…O13	0.0256	0.0775	−0.1145 0.10^{-3}	−0.0196	51.41
	N10-H6…O11	0.0290	0.0912	−0.1751 0.10^{-3}	−0.0231	60.59
2	N8-H3…O13	0.0139	0.0445	0.0002	−0.0107	28.06
	N9-H6…O13	0.0267	0.0742	−0.8114. 10^{-3}	−0.0201	52.72
	O16-H17…O12	0.0380	0.1122	0.1598. 10^{-3}	−0.0278	72.92
	O13-H14…O16	0.0390	0.1171	−0.1390. 10^{-4}	−0.0293	76.85
	N10-H6…O11	0.0288	0.0898	−0.2422. 10^{-3}	−0.0229	60.06
3	N14-H9…O19	0.0211	0.0807	0.0025	−0.0151	39.6
	N15-*H*11…O19	0.0226	0.0792	0.0019	−0.0159	41.7
	N16-H12…O17	0.0290	0.1103	0.0021. 10^{-2}	−0.0233	61.11
	O19-H21…O1	0.0421	0.1347	−0.0026	−0.0388	101.77
	O1-H3…O4	0.0411	0.1347	−0.0020	−0.0376	98.62
	O4-H6…O18	0.0367	0.1308	−0.1208. 10^{-3}	−0.0329	86.29
4	N18-H3…O19	0.0216	0.0654	−0.2954. 10^{-3}	−0.0169	44.32
	O19-H20…O13	0.0289	0.0847	−0.3305. 10^{-3}	−0.0218	57.18
	N9-H5…O19	0.0300	0.0822	−0.0012	−0.0220	57.7
	O19-H21…O16	0.0313	0.0913	−0.3356. 10^{-3}	−0.0230	60.32
	O13-H15…O22	0.0308	0.0903	−0.1315. 10^{-3}	−0.0220	57.7
	O22-H24…O12	0.0487	0.1459	−0.8494. 10^{-3}	−0.0381	99.9
	N10-H6…O11	0.0308	0.0960	−0.2685. 10^{-3}	−0.0240	62.95
5	N16-H12…O17	0.0307	0.0956	−0.2765. 10^{-3}	−0.0244	64
	N15-*H*11…O4	0.0321	0.0857	−0.0012	−0.0238	62.42
	N14-H9…O4	0.0195	0.0597	−0.1891. 10^{-3}	−0.0153	40.13
	O4-H5…O22	0.2451	0.0710	−0.4564. 10^{-3}	−0.0186	48.78
	O25-H27…O19	0.0398	0.1139	−0.5233. 10^{-3}	−0.0295	77.37
	O1-H3…O18	0.0361	0.1113	0.4838. 10^{-3}	−0.0268	70.29
	O19-H20…O18	0.0232	0.0677	−0.0360. 10^{-3}	−0.0176	46.16
	O22-H24…O1	0.0402	0.1195	−0.1286. 10^{-3}	−0.0299	78.42
	O4-H6…O25	0.0349	0.1053	0.1354. 10^{-3}	−0.0260	68.19
6	N17-H12…O7	0.0140	0.0447	0.1762. 10^{-3}	−0.0108	28.32
	N18-H14…O7	0.0358	0.0693	−0.0011. 10^{-3}	−0.0265	69.51
	O28-H30…O21	0.0284	0.0864	0.2467. 10^{-3}	−0.0211	55.34
	O22-H24…O21	0.0220	0.0608	−0.7184. 10^{-3}	−0.0166	43.54
	O1-H2…O4	0.0355	0.0141	−0.1166. 10^{-3}	−0.0262	68.72
	O4-H6…O28	0.0523	0.1407	−0.0029	−0.0411	107.80
	O25-H27…O1	0.0408	0.1197	−0.1788. 10^{-3}	−0.0302	79.21
	O7-H8…O22	0.0337	0.0941	−0.7059. 10^{-3}	−0.0249	65.31
	O7-H9…O4	0.0259	0.0472	−0.5059. 10^{-3}	−0.0195	51.14
	O28-H29…O25	0.0256	0.0736	−0.5354. 10^{-3}	−0.0194	50.88
	O22-H23…O25	0.0254	0.0740	−0.4054. 10^{-3}	−0.0193	50.62
	O22-H23…O21	0.0220	0.0608	−0.0718. 10^{-3}	−0.0166	43.54
7	N17-H12…O7	0.0200	0.0607	−0.2761. 10^{-3}	−0.0157	41.18
	N18-H14…O7	0.0322	0.0877	−0.0010	−0.0204	53.50
	N19-H15…O20	0.0302	0.0940	−0.2657. 10^{-3}	−0.0240	62.95
	O4-H5…O21	0.0272	0.0817	0.7739. 10^{-3}	−0.0202	52.98
	O22-H23…O21	0.0272	0.0818	0.7847. 10^{-3}	−0.0202	52.98
	O31-H33…O4	0.0501	0.1372	−0.0022	−0.0388	101.77
	O4-H6…O28	0.0275	0.0800	−0.3986. 10^{-3}	−0.0208	54.55
	O22-H24…O28	0.0275	0.0799	−0.3995. 10^{-3}	−0.0207	54.29
	O25-H27…O31	0.0269	0.0768	−0.5550. 10^{-3}	−0.0203	53.24
	O1-H2…O22	0.0501	0.1372	−0.0022	−0.0388	101.77
	O25-H26…O1	0.0268	0.0767	−0.5565. 10^{-3}	−0.0202	52.98
	O7-H9…O1	0.0306	0.0893	−0.2426. 10^{-3}	−0.0228	59.80
8	N20-H15…O10	0.0228	0.0688	−0.3425. 10^{-3}	−0.0178	46.68
	N21-H17…O10	0.0290	0.0786	−0.0010	−0.0217	56.91
	N22-H18…O23	0.0309	0.0963	−0.2652. 10^{-3}	−0.0246	64.52
	O1-H2…O24	0.0279	0.0853	0.2338. 10^{-3}	−0.0208	54.55
	O4-H5…O24	0.0263	0.0816	0.2973. 10^{-3}	−0.0198	51.93
	O10-H12…O34	0.0305	0.0897	−0.8836. 10^{-4}	−0.0226	59.28
	O10-*H*11…O7	0.0315	0.0928	−0.1378. 10^{-3}	−0.0234	61.37
	O31-H32…O34	0.0292	0.0830	−0.4410. 10^{-3}	−0.0216	56.65
	O31-H33…O7	0.0273	0.0782	−0.5124. 10^{-3}	−0.0205	53.77
	O25-H27…O31	0.0483	0.1337	−0.0017	−0.0369	96.78
	O1-H3…O25	0.0280	0.0810	−0.4246. 10^{-3}	−0.0211	55.34
	O4-H6…O25	0.0296	0.0863	−0.2494. 10^{-3}	−0.0220	57.70
	O34-H35…O28	0.0494	0.1429	−0.0014	−0.0385	100.98
	O28-H29…O4	0.0492	0.1378	−0.0017	−0.0380	99.67
	O7-H9…O1	0.0518	0.1404	−0.0027	−0.0406	106.49
9	N20-H15…O25	0.0214	0.0641	−0.3824. 10^{-3}	−0.0168	44.06
	N21-H17…O25	0.0372	0.1023	−0.0010	−0.0277	72.65
	N22-H18…O23	0.0309	0.0959	−0.3016. 10^{-3}	−0.0245	64.26
	O4-H6…O24	0.0379	0.1168	0.5208. 10^{-3}	−0.0281	73.70
	O28-H30…O24	0.0273	0.0809	−0.3776. 10^{-3}	−0.0203	53.24

Table 9 (*continued*)

	H-bonds	ρ	Δρ	H	V_{BCP}	$E_{H\ldots O}$
	O28-H29…O34	0.0285	0.0812	−0.4496. 10^{-3}	−0.0212	55.60
	O25-H27…O34	0.0303	0.0887	−0.1957. 10^{-3}	−0.0225	59.01
	O37-H38…O4	0.0286	0.0829	−0.2831. 10^{-3}	−0.0213	55.87
	O1-H3…O10	0.0272	0.0774	−0.5441. 10^{-3}	−0.0204	53.50
	O10-*H*11…O37	0.0502	0.1374	−0.0023	−0.0389	102.03
	O31-H32…O10	0.0296	0.0851	−0.3996. 10^{-3}	−0.0220	57.70
	O31-H33…O7	0.0268	0.0765	−0.5232. 10^{-3}	−0.0201	52.72
	O37-H39…O7	0.0306	0.0899	−0.1787. 10^{-3}	−0.0228	59.80
	O7-H9…O28	0.0502	0.1394	−0.0021	−0.0391	102.56
	O34-H36…O31	0.0511	0.1396	−0.0025	−0.0399	104.65
	O25-H26…O1	0.0402	0.1153	−0.5262. 10^{-3}	−0.0298	78.16
10	N25-H21…O26	0.0294	0.0917	−0.2402. 10^{-3}	−0.0234	61.37
	N24-H20…O13	0.0243	0.0718	−0.4222. 10^{-3}	−0.0158	41.44
	N23-H18…O13	0.0157	0.0455	−0.2542. 10^{-3}	−0.0118	30.95
	O10-*H*11…O27	0.0229	0.0675	−0.1948. 10^{-3}	−0.0172	45.11
	O37-H38…O27	0.0270	0.0779	−0.5162. 10^{-3}	−0.0205	53.77
	O37-H39…O40	0.0213	0.0658	−0.1644. 10^{-3}	−0.0167	43.80
	O40-H42…O34	0.0246	0.0717	−0.5626. 10^{-3}	−0.0190	49.83
	O4-H6…O1	0.0261	0.00786	−0.2814. 10^{-3}	−0.0202	52.98
	O28-H29…O10	0.0216	0.0679	−0.1086. 10^{-3}	−0.0172	45.11
	O13-H15…O31	0.0302	0.0879	−0.3318. 10^{-3}	−0.0226	59.28
	O4-H5…O31	0.0248	0.0700	−0.6309. 10^{-3}	−0.0187	49.05
	O28-H30…O34	0.3371	1.8245	−0.5043. 10^{-3}	−0.5525	1449.22
	O40-H41…O10	0.0372	0.1045	−0.7301. 10^{-3}	−0.0275	72.13
	O13-H14…O1	0.0423	0.1175	−0.0010	−0.0315	82.62
	O1-H2…O7	0.0347	0.1032	−0.1245. 10^{-3}	−0.0260	68.19
	O7-H9…O37	0.0394	0.1133	−0.3466. 10^{-3}	−0.0203	53.24
	O34-H35…O4	0.0464	0.1282	−0.0014	−0.0350	91.80

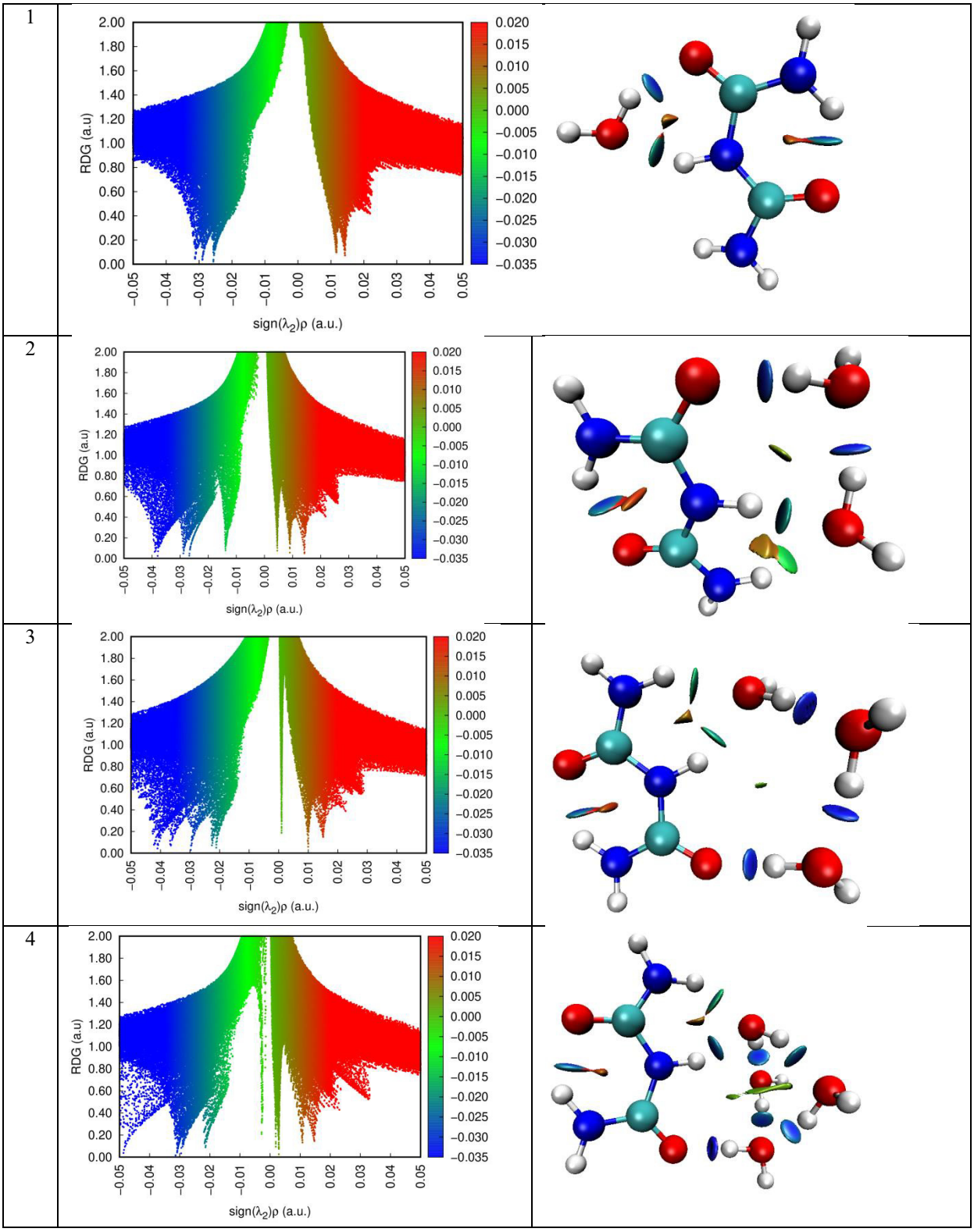

Fig. 8. RDG map along with VMD representation of the different clusters.

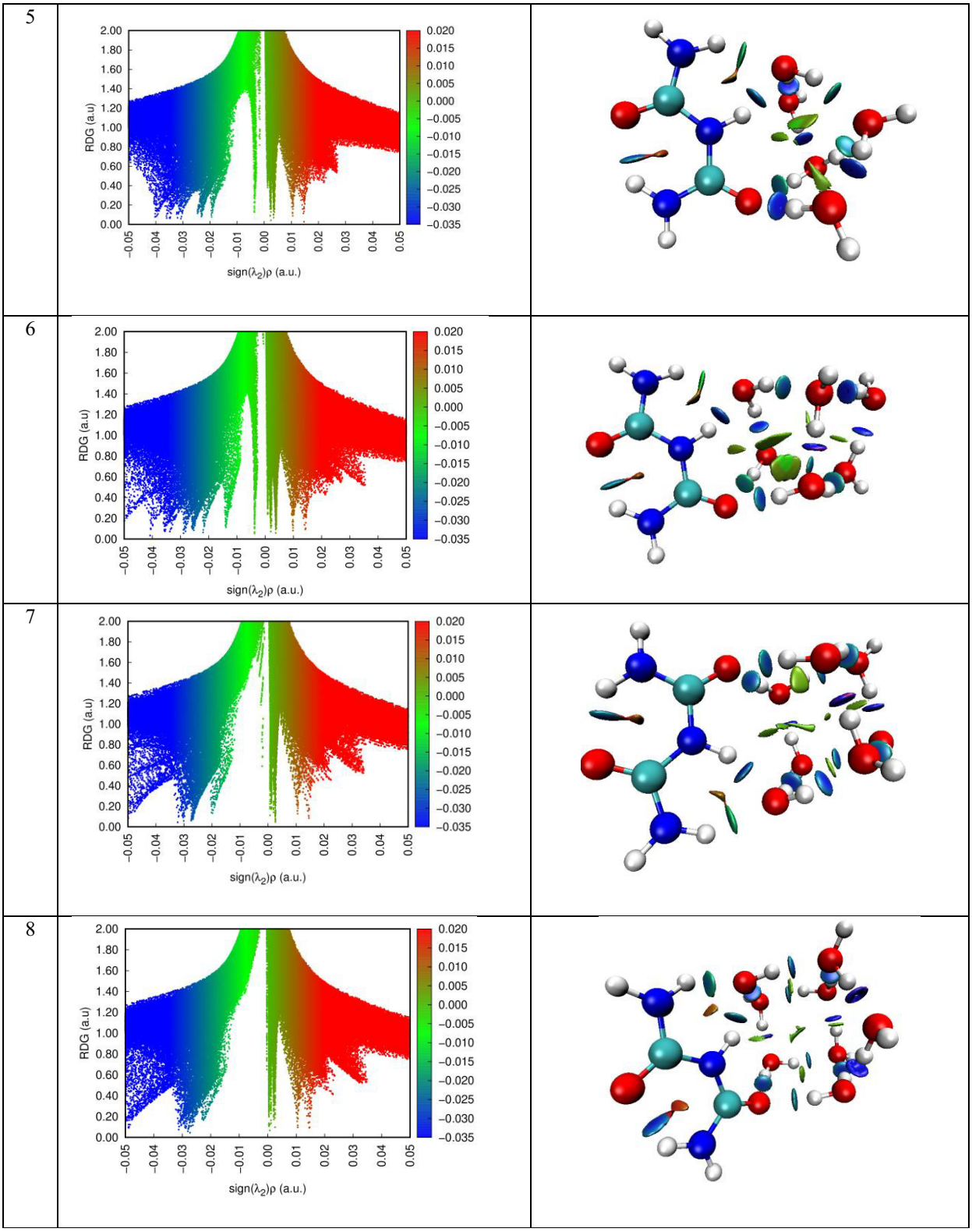

Fig. 8 (*continued*)

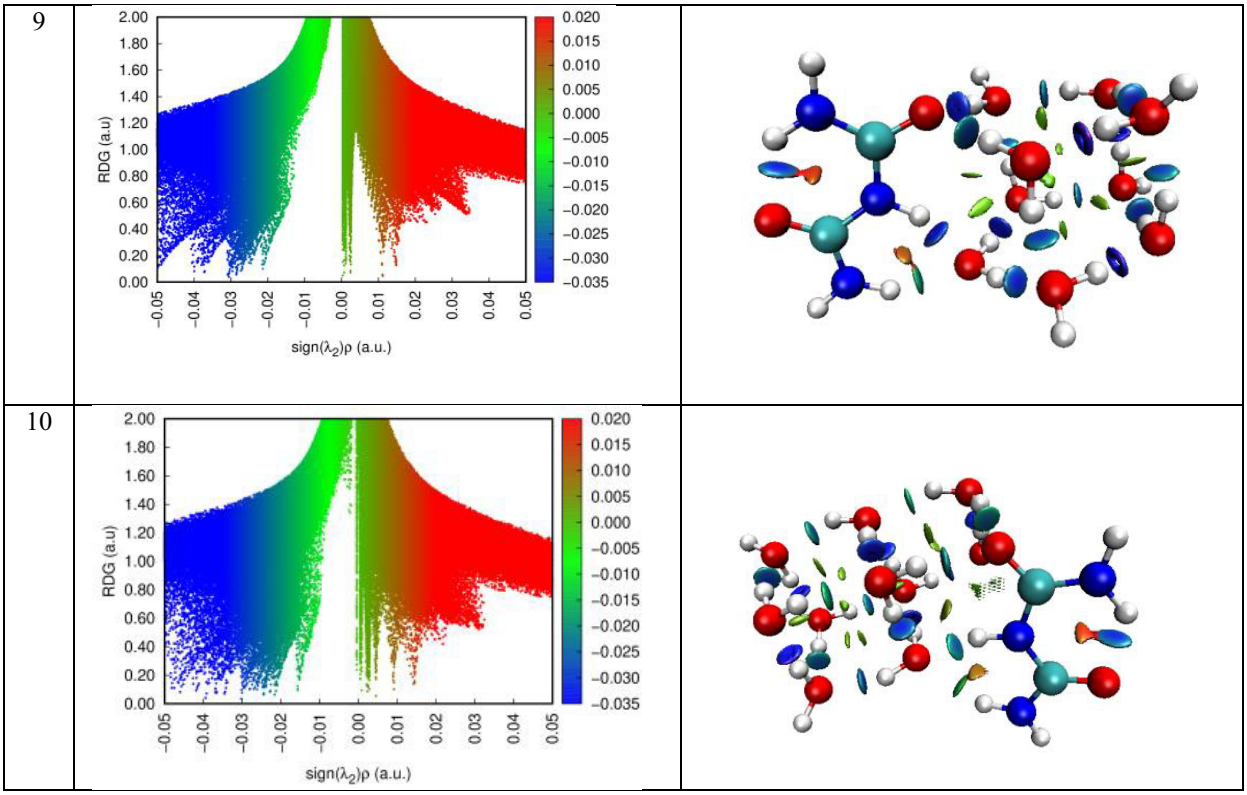

Fig. 8 (*continued*)

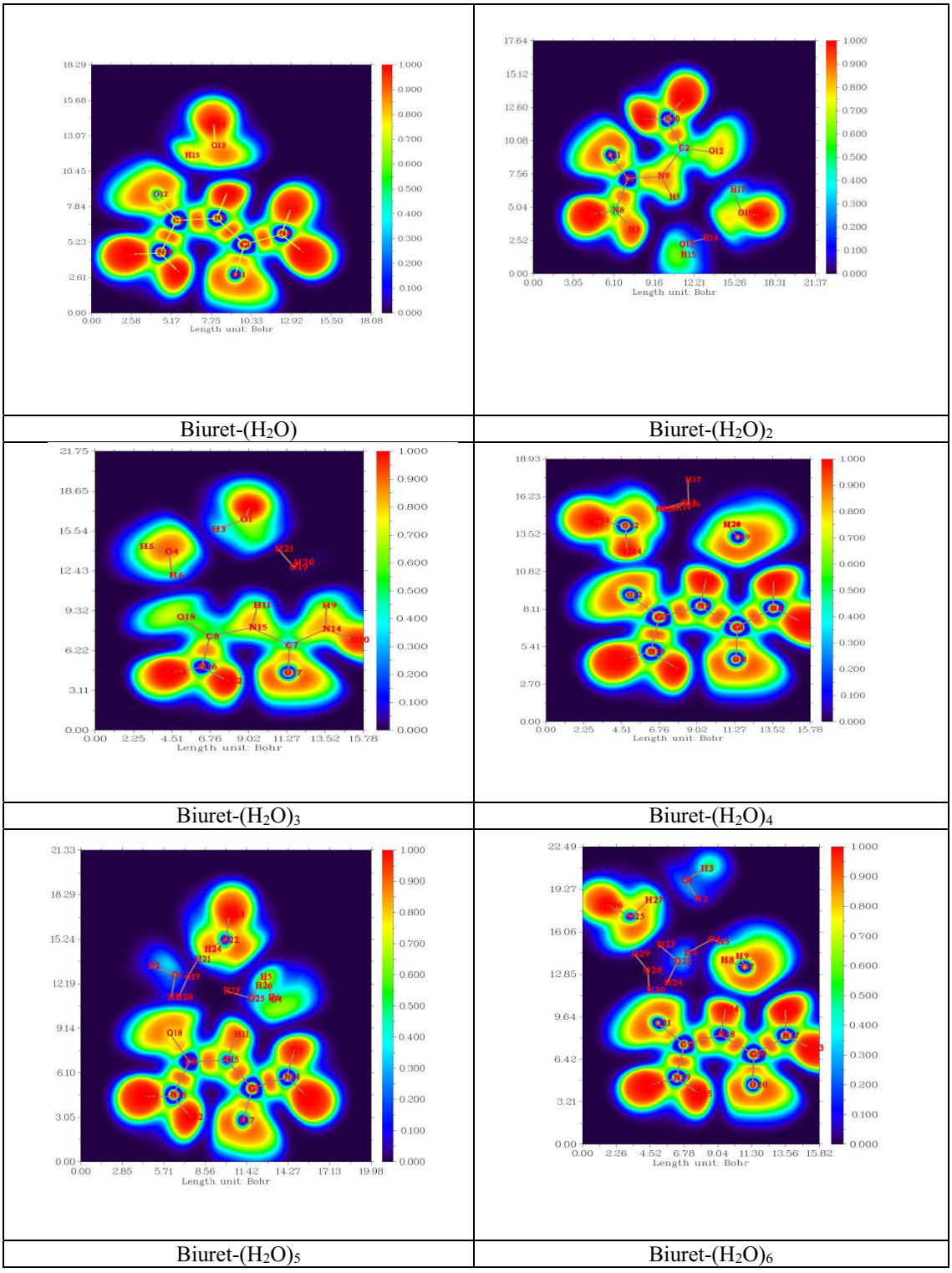

Fig. 9. 2D ELF representation of Biuret-water clusters.

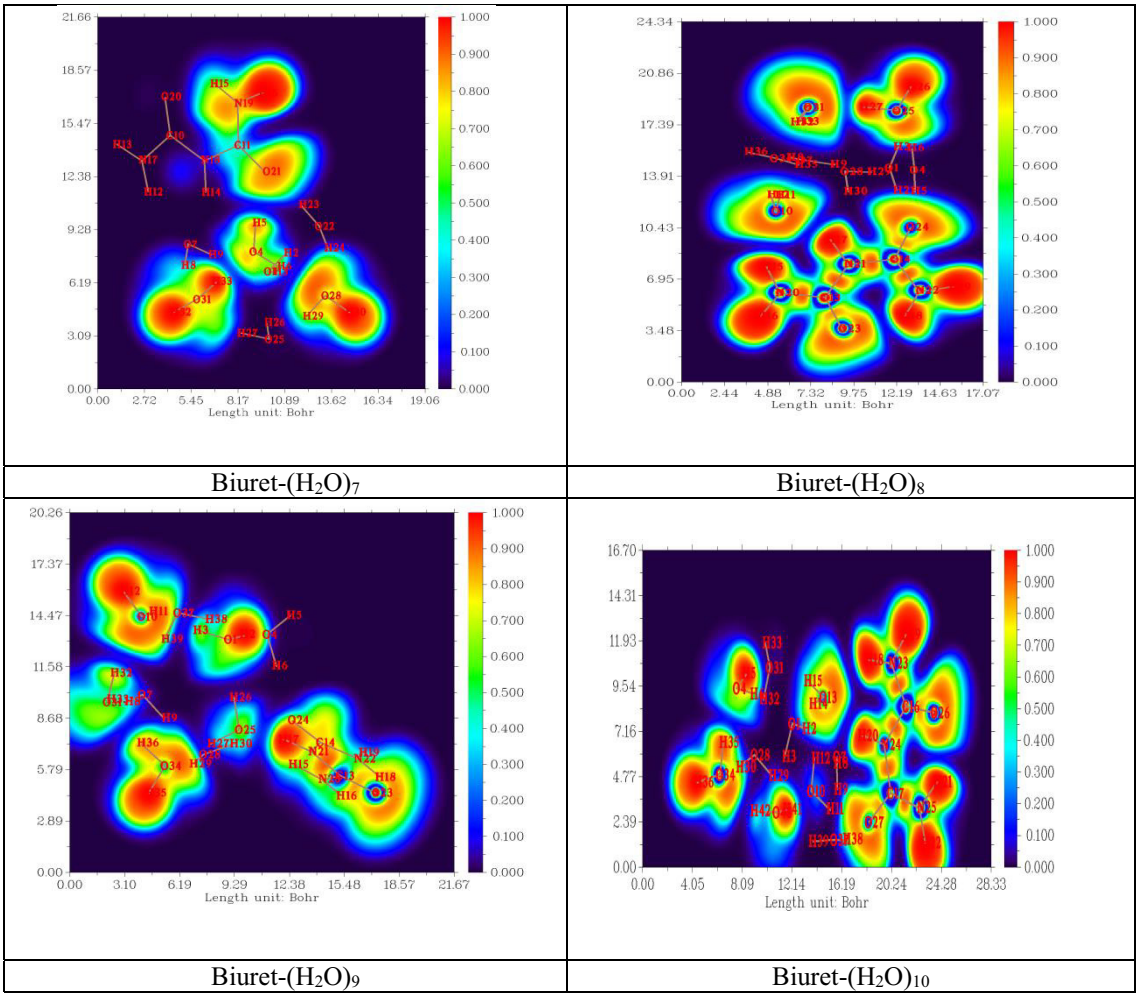

Fig. 9 (*continued*)

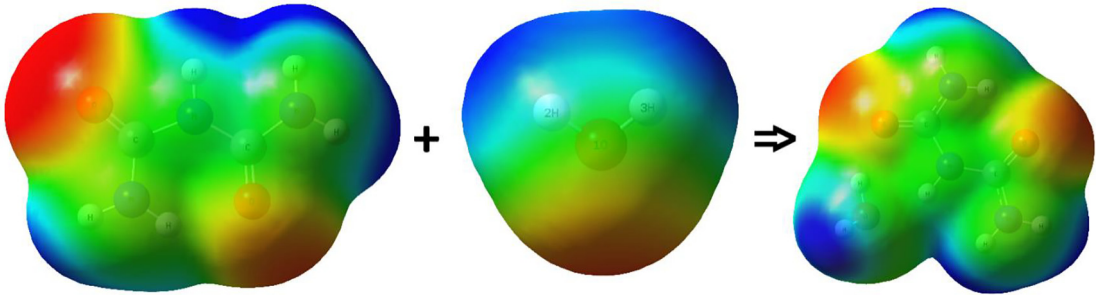

Fig. 10. The electrostatic potential (ESP) analysis of biuret, water and biuret-water cluster (with 1 water molecule).

References

Akman, F., Issaoui, N., Kazachenko, A.S., 2020. Intermolecular hydrogen bond interactions in the thiourea/water complexes (Thio-(H2O)n) (n = 1, 5): X-ray, DFT, NBO, AIM, and RDG analyses. J. Mol. Model. 26, 161. https://doi.org/10.1007/s00894-020-04423-3.

Bader, R.F.W., 1990. Atoms in Molecules – A Quantum Theory. Oxford University Press, Oxford.

Becke, A.D., Edgecombe, K.E., 1990. A simple measure of electron localization in atomic and molecular systems. J. Chem. Phys. 92, 5397–5403.

Bernhard, A.M., Peitz, D., Elsener, M., Wokaun, A., Kröcher, O., 2012. Hydrolysis and thermolysis of urea and its decomposition byproducts biuret, cyanuric acid and melamine over anatase TiO2. Appl. Catal. B. 115–116, 129–137. https://doi.org/10.1016/j.apcatb.2011.12.013.

Carr, J.K., Buchanan, L.E., Schmidt, J.R., Zanni, M.T., Skinner, J.L., 2013. Structure and dynamics of urea/water mixtures investigated by vibrational spectroscopy and molecular dynamics simulation. J. Phys. Chem. B. 117 (42), 13291–13300.

Contreras Aguilar, E., Echeverría, G.A., Piro, O.E., Ulic, S.E., Jios, J.L., Tuttolomondo, M. E., Molina, R.D.I., Arena, M.E., 2019. Acyl thiourea derivatives: A study of crystallographic, bonding, biological and spectral properties. Chem. Phys. Lett. 715, 64–71.

Dennington, R., Keith, T., Millam, J., 2010. GaussView, Version 5. Semichem Inc., Shawnee Mission KS.

Dong, F., Wu, L., Sun, Y., Fu, M., Wu, Z., Lee, S.C., 2011. Efficient synthesis of polymeric g-C3N4 layered materials as novel efficient visible light driven photocatalysts. J. Mater. Chem. 21, 15171–15174. https://doi.org/10.1039/C1JM12844B.

Drissi, M., Benhalima, N., Megrouss, Y., Rachida, R., Chouaih, A., Hamzaoui, F., 2015. Theoretical and Experimental Electrostatic Potential around the m-Nitrophenol

Molecule. Molecules. 20 (3), 4042–4054. https://doi.org/10.3390/molecules20034042.
Fazilath Basha, A., Liakath Ali Khan, F., Muthu, S., Raja, M., 2021. Computational evaluation on molecular structure (Monomer, Dimer), RDG, ELF, electronic (HOMO-LUMO, MEP) properties, and spectroscopic profiling of 8-Quinolinesulfonamide with molecular docking studies. Computat. Theoret. Chem. 1198, 113169.
Fleming, I., 1976. Frontier Orbitals and Organic Chemical Reactions. Wiley, London.
Fonnesbeck, P.V., Kearl, L.C., Harris, L.E., 1975. Feed Grade Biuret as a Protein Replacement for Ruminants. A Review. J. Animal Science. 40, 1150–1184. https://doi.org/10.2527/jas1975.4061150x.
M.J. Frisch, G.W. Trucks, H.B. Schlegel, Gaussian 09, Revision D.01,(2013) Gaussian Inc., Wallingford.
Fuster, F., Sevin, A., Silvi, B., 2000. Topological Analysis of the Electron Localization Function (ELF) Applied to the Electrophilic Aromatic Substitution. J. Phys. Chem. A 104 (4), 852–858. https://doi.org/10.1021/jp992783k.
Gatfaoui, S., Issaoui, N., Roisnel, T., Marouani, H., 2019. A proton transfer compound template phenylethylamine: Synthesis, a collective experimental and theoretical investigations. J. Mol. Struct. 1191, 183–196. https://doi.org/10.1016/j.molstruc.2019.04.093.
Melek Hajji, Jamelah S. Al-Otaibi, Marwa Belkhiria, Selma Dhifaoui, Mohamed A. Habib, Salima Moftah H Elmgirhi, Hasan Mtiraoui, Radhouane Bel-Hadj-Tahar, Moncef Msaddek, Taha Guerfel, Structural and computational analyses of a 2-propanolammonium-chlorocadmate(II) assembly: Pivotal role of hydrogen bonding and H—H interactions, J. Molecul. Struct., 1223, 2021, 128998.
Hajji, M., Abad, N., Habib, M.A., Salima, M.H., Elmgirhi,, 2021. Taha Guerfel, Computational chemistry methods for modelling non-covalent interactions and chemical reactivity— An overview. J. Indian Chem. Soc. 98, (11) 100208.
Hammami, F., Ghalla, H., Nasr, S., 2015. Intermolecular hydrogen bonds in urea-water complexes: DFT, NBO, and AIM analysis. Comput. Theor. Chem. 1070, 40–47.
Hughes, E.W., Yakel, H., Freeman, H.C., 1961. The Crystal Structure of Biuret Hydrate. Acta Crystallogr. 14, 345–352. https://doi.org/10.1107/S0365110X61001194.
Johnson, E.R., Keinan, S., Mori-Sanchez, P., Contreras-Garcia, J., Cohen, A.J., Yang, W. T., 2010. J. Am. Chem. Soc. 132, 6498–6506.
Kazachenko, A.S., Akman, F., Abdelmoulahi, H., Issaoui, N., Malyar, Y.N., Al-Dossary, O., Wojcik, M.J., 2021. Intermolecular hydrogen bonds interactions in water clusters of ammonium sulfamate: FTIR, X-ray diffraction, AIM, DFT, RDG, ELF, NBO analysis. J. Molecul. Liquids. 342, 117475.
Kazachenko, A.S., Malyar, Y.N., Vasilyeva, N.Y., Borovkova, V.S., Issaoui, N., 2021. Optimization of guar gum galactomannan sulfation process with sulfamic acid. Biomass Convers. Biorefin. https://doi.org/10.1007/s13399-021-01895-y.
Kazachenko, A.S., Akman, F., Sagaama, A., Issaoui, N., Malyar, Y.N., Vasilieva, N.Y., Borovkova, V.S., 2021. Theoretical and experimental study of guar gum sulfation. J. Mol. Model 27, 5. https://doi.org/10.1007/s00894-020-04645-5.
Kazachenko, A.S., Medimagh, M., Issaoui, N., Al-Dossary, O., Wojcik, M.J., Kazachenko, A.S., Miroshnokova, A.V., Malyar, Y.N., 2022. Sulfamic acid/water complexes (SAA-H2O(1–8)) intermolecular hydrogen bond interactions: FTIR, X-ray, DFT and AIM analysis. J. Molecul. Struct. 1265, 133394.
Koebel, M., Elsener, M., Kleemann, M., 2000. Urea-SCR: a promising technique to reduce NOx emissions from automotive diesel engines. Catal. Today. 59, 335–345. https://doi.org/10.1016/S0920-5861(00)00299-6.
B. Kunkle, J. Fletcher, D. Mayo. Florida Cow-Calf Management, 2nd Edition - Feeding the Cow Herd. IFAS Extension, University of Florida. Publication #AN117. (2013).
Liu, J., Zhang, T., Wang, Z., Dawson, G., Chen, W., 2011. Simple pyrolysis of urea into graphitic carbon nitride with recyclable adsorption and photocatalytic activity. J. Mater. Chem. 21, 14398–14401. https://doi.org/10.1039/C1JM12620B.
Lovrinčević, B., Požar, M., Balić, M., 2020. Dynamics of urea-water mixtures studied by molecular dynamics simulation. J. Molecul. Liquid. 300.
Lu, T., Chen, F., 2012. Multiwfn: a multifunctional wavefunction analyzer. J. Comput. Chem. 33 (5), 580–592. https://doi.org/10.1002/jcc.22885.
Ludwig, R., 2001. Water: From Clusters to the Bulk. Angew. Chem. Int. Ed. 40 (10), 1808–1827. https://doi.org/10.1002/1521-3773(20010518)40:10<1808::AID-ANIE1808>3.0.CO;2-1.
Michalski, M., Gordon, A.J., Berski, S., 2019. Topological analysis of the electron localisation function (ELF) applied to the electronic structure of oxaziridine: the nature of N-O bond. Struct. Chem. 30, 2181–2189. https://doi.org/10.1007/s11224-019-01407-9.
Nicolaou, K.C., Bulger, P.G., Sarlah, D., 2005. Palladium-Catalyzed Cross-Coupling Reactions in Total Synthesis. Angew. Chem. Int. Ed. 44, 4442–4489. https://doi.org/10.1002/anie.200500368.
Noureddine, O., Issaoui, N., Medimagh, M., Al-Dossary, O., Marouani, H., 2021. Quantum chemical studies on molecular structure, AIM, ELF, RDG and antiviral activities of hybrid hydroxychloroquine in the treatment of COVID-19: Molecular docking and DFT calculations. J. King Saud Univers. – Sci. 33 (2), 101334.
Oltjen, R.R., Williams, E.E., Slyter, L.L., Richardson, G.V., 1969. Urea versus biuret in a roughage diet for steers. J. Animal Science. 29, 816–822. https://doi.org/10.2527/jas1969.295816x.
Petersson, G.A., Al-Laham, M.A., 1991. A complete basis set model chemistry. II. Open-shell systems and the total energies of the first-row atoms. J. Chem. Phys. 94 (9), 6081–6090.
Petersson, G.A., Bennett, A., Tensfeldt, T.G., Al-Laham, M.A., Shirley, W.A., Mantzaris, J., 1988. A complete basis set model chemistry. I. The total energies of closed-shell atoms and hydrides of the first-row elements. J. Chem. Phys. 89 (4), 2193–2218.
Sharma, D., Tiwari, S.N., 2016. Comparative computational analysis of electronic structure, MEP surface and vibrational assignments of a nematic liquid crystal: 4-n-methyl-4́-cyanobiphenyl. J. Mol. Liq. 214, 128–135. https://doi.org/10.1016/j.molliq.2015.11.045.
Supriya, S., Das, S.K., 2003. Small Water Clusters in Crystalline Hydrates. J. Clust. Sci. 14, 337–366. https://doi.org/10.1023/B:JOCL.0000005068.77622.a4.
Timmer, B.J.J., Mooibroek, T.J., 2021. Intermolecular π–π Stacking Interactions Made Visible. J. Chem. Educ. 98 (2), 540–545. https://doi.org/10.1021/acs.jchemed.0c01252.
Udachin, K., Alavi, S., Ripmeester, J.A., 2011. Communication: Single crystal x-ray diffraction observation of hydrogen bonding between 1-propanol and water in a structure II clathrate hydrate. J. Chem. Phys. 134, (12). https://doi.org/10.1063/1.3574393 121104.
Udupa, M.R., Indira, V., 1975. Biuret complexes of copper(II) and nickel(II). J. Indian Chem. Soc. 52, 585–588.
Uno, T., Machida, K., 1962. Infrared spectra of succinimide and maleimide in the crystalline state. Bull. Chem. Soc. Japan 35, 276–283.
Volz, N., Clayden, J., 2011. The Urea Renaissance. Angew. Chem. Int. Ed. 50, 12148–12155. https://doi.org/10.1002/anie.201104037.
Wang, S.L., Zhang, L.Y., Jiang, F., Huang, Q., 2015. Synthesis, Structures and Properties of Two New Coordination Polymers with Unprecedented Water Cluster. J. Clust. Sci. 26 (3), 959–972.
Wang, M.-L., Zhong, G.-Q., Chen, L., 2016. Synthesis, Optical Characterization, and Thermal Decomposition of Complexes Based on Biuret Ligand. Int. J. Optics, 1–8. https://doi.org/10.1155/2016/5471818.
Yadav, S., Nawani, S., Goel, N., 2017. Ozone-Water Interaction Revisited Through $[(O_3)_m\cdots(H_2O)_n]$ Clusters. J. Clust. Sci. 28, 1693–1708. https://doi.org/10.1007/s10876-017-1177-1.
Yokoya, M., Kimura, S., Yamanaka, M., 2021. Urea Derivatives as Functional Molecules: Supramolecular Capsules, Supramolecular Polymers, Supramolecular Gels, Artificial Hosts, and Catalysts. Chem. Eur. J. 27, 5601–5614. https://doi.org/10.1002/chem.202004367.
Zhang, J., Dolg, M., 2015. ABCluster: the artifcial bee colony algorithm for cluster global optimization. Phys. Chem. Chem. Phys. 17 (37), 24173–122418. https://doi.org/10.1039/C5CP04060D.
Zumdahl, S.S., 2000. Chemistry for Chemical and Biological Sciences. University Science Books, Sausalito, CA.